CA3 circuit model compressing sequential information in theta oscillation and replay

Satoshi Kuroki, Kenji Mizuseki

Department of Physiology, Osaka Metropolitan University Graduate School of Medicine, Asahimachi 1-4-3, Abeno-ku, Osaka, 545-8585, Japan
skuroki@omu.ac.jp

Abstract

The hippocampus compresses the sequential information in a theta oscillation cycle and short-term sequential activities during sharp-wave ripple in sleep or rest, processes known as theta sequence and replay, respectively. The theta sequence is based on theta phase precession patterns of individual neurons. It is, however, still unknown how these sequential neuronal activities are generated and store information about the outside environment. To address this, we developed a hippocampal CA3 computational model based on anatomical and electrophysiological evidence of the biological CA3 circuit. The model consists of theta rhythm inhibition, place input, and CA3-CA3 plastic recurrent connection. The model was able to compress the sequence of the external inputs and reproduce theta phase precession and replay, learn additional sequences, and reorganize previously learned sequences. The mechanism of sequence acquisition was explained by a gradual increase of synaptic inputs. This model hypothesizes how the CA3 circuit acquires, compresses, and replays sequential information.

Introduction

The hippocampus contributes to forming episodic memory (Gordon, 1988; Scoville and Milner, 1957). Rodent spatial memory has been extensively studied as a model for episodic memory (O'Keefe and Dostrovsky, 1971; O'keefe and Nadel, 1978; Tolman, 1948). In the hippocampus, individual place information is represented as phase code within theta cycles of local field potential (LFP) through a phenomenon known as theta phase precession, where firing timings within theta oscillations advance as one progresses. Consequently, sequential activity is manifested as firing order within a theta cycle, forming theta sequences. (O'Keefe and Recce, 1993; Skaggs et al., 1996). The sequential activities are replayed during sharp-wave ripple

(SWR) during sleep and quiet resting (Diba and Buzsáki, 2007; Foster and Wilson, 2006). It has been hypothesized that sequential activity compresses relationships in the external world in the order of seconds to minutes into neural sequences in the order of ten to hundred milliseconds, and it enables more efficient processing, storage, and retrieval of information, as well as integrating information into cognitive processes such as memory consolidation, abstraction, planning, and inference (Buzsáki, 2015; Drieu and Zugaro, 2019).

The hippocampus can be divided into several subregions, mainly Dentate Gyrus (DG), Cornu Ammonis 1 and 3 (CA1 and CA3), each of which plays an important and distinct role in episodic and place memory. In particular, the CA3 is an important part of generating the sequential activity. The CA3 is a starting point of the ripple (Buzsáki, 1986; Buzsáki et al., 1983; Suzuki and Smith, 1988) and replay (Middleton and McHugh, 2016) activities. The CA3 receives input from the DG and projects to the CA1. Input from the DG is very sparse in the CA3, but each input strength is large (Henze et al., 2002, 2000). In the CA3, there are more recurrent connections between the excitatory neurons than those in the DG and the CA1. Synapses between CA3 excitatory neurons are weaker with a higher connection probability than those from DG to CA3 excitatory neurons. Both DG-CA3 and CA3-CA3 synapses show short- and long-term plasticity (Rebola et al., 2017). These anatomical features of CA3 circuits seem optimal for sequence learning (Banino et al., 2018; Jaeger and Haas, 2004; Laje and Buonomano, 2013; Sussillo and Abbott, 2009; Wang et al., 2018).

Inhibitory cells in the hippocampus control the synchronization in the entire hippocampus by receiving theta-modulated inputs from GABAergic neurons of the Medial Septum (MS), then control the firing timing of the excitatory cells (Freund and Antal, 1988; King et al., 1998; Petsche et al., 1962; Zutshi et al., 2018). Inhibitory cells also receive input from nearby excitatory cells and send them feedback inhibition (Rebola et al., 2017).

Several computational models for the generation of theta phase precessions (Chadwick et al., 2016; Geisler et al., 2010) and for the compression of sequences (Ecker et al., 2022; Jahnke et al., 2015; Nicola and Clopath, 2019; Reifenstein et al., 2021) were proposed. There is still, however, no model that explains all these phenomena unified. Therefore, this paper focuses on the CA3 structure, which has many recurrent connections and is a source of SWRs, as a critical region to acquire the sequence compression, and presents a mathematical model of how CA3 can memorize and replay the order of external place sequence.

Results

We developed a minimal CA3 neural network based on anatomical evidence to understand the fundamental mechanisms by which the CA3 recurrent circuit compresses sequential information (Figure 1A). The network consists of eight excitatory and one inhibitory neural unit. The excitatory neural units receive three inputs from DG, CA3 recurrent, and the inhibitory unit. DG input is sparse and large in the biological brain (Henze et al., 2002, 2000). The activity of DG is also very sparse and makes the input pattern separated more clearly, named pattern separation (Yassa and Stark, 2011). To simplify the network, we assumed that each CA3 excitatory unit

received only one DG input, but the synaptic weight was large (Figure 1A). Half of the DG inputs had place fields (the order of unit #1-2-3-4) and the others were silent (Figure 1B). The CA3 excitatory units were connected to each other, and the recurrent synapses were plastic. The CA3 excitatory units also received feedback inhibition from the CA3 inhibitory unit. The inhibitory neuron received excitatory inputs from CA3 excitatory units and inhibitory theta inputs from MS (Freund and Antal, 1988; King et al., 1998; Petsche et al., 1962; Zutshi et al., 2018) (Figure 1A and C). We tested whether the network model can learn sequential activity within the network by experiencing the place order and whether it replays the sequence without the external inputs.

In this model, we set plasticity only in CA3 recurrent synapses and did not set it in DG-CA3 synapses to simplify the learning process. We selected the CA3 recurrent synapses because recurrent networks like CA3-CA3 connections, are suitable for learning sequential activities (Banino et al., 2018; Jaeger and Haas, 2004; Laje and Buonomano, 2013; Sussillo and Abbott, 2009; Wang et al., 2018). The plasticity rule was Hebbian. Activated synapses are tagged much longer than membrane potential changes (referred plasticity-related factor, see Material and Methods) (Rogerson et al., 2014), which makes sequence learning with the Hebbian rule more efficient (Reifenstein et al., 2021). Furthermore, when inputs from DG and another CA3 neuron come simultaneously, the neuronal response is much higher than the simple summation of the responses to these two inputs called superlinear coincident detection (Brandalise and Gerber, 2014; London and Häusser, 2005). We implemented these synaptic properties into the model (see Materials and Methods). We also added the regularization term of the synaptic weight (maintaining summation of postsynaptic weights as a constant same value, see Materials and Methods) to prevent overexcitation. The self-connection in the CA3-CA3 recurrent synapses was excluded.

The model was assumed to run on linear space with constant velocity (1 cm/s) for 10 trials (running session). During the running session, the plasticity on the CA3-CA3 recurrent synapse was working and changing the synaptic weights. Figure 1D-F shows CA3 unit spikes (Figure 1D and E) and membrane potentials (Figure 1F) of both excitatory and inhibitory units in the first, middle, and last trials. Note that firing starts timing became earlier according to the trial processes. The new spikes were generated because of the synaptic weight changes in the CA3-CA3 recurrent synapse.

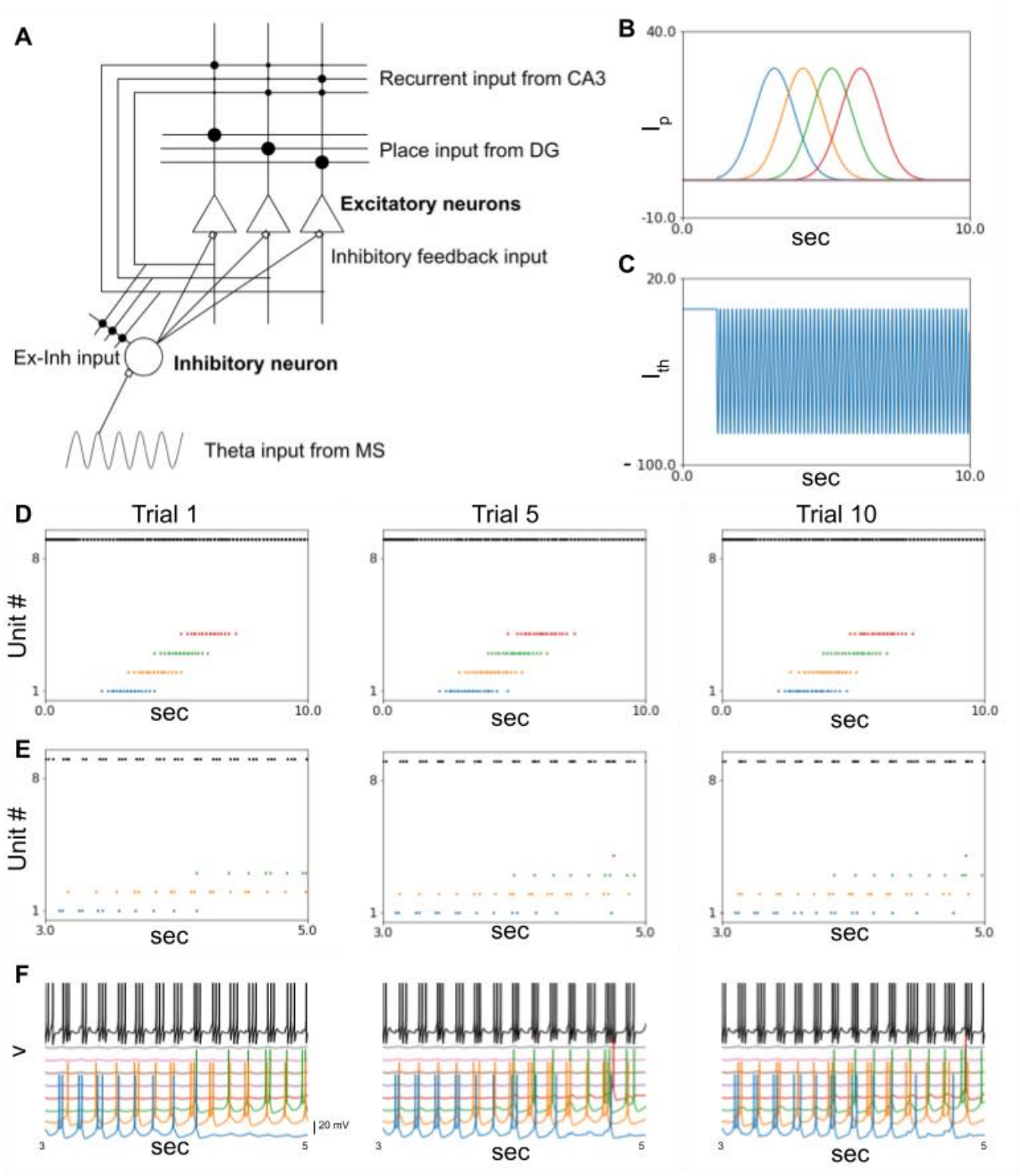

Figure 1 Small CA3 model

(A) Schematic figure of model construction. The white triangle indicates the CA3 pyramidal neuronal unit and the large white circle indicates the CA3 inhibitory neuronal unit. Lines indicate axons and dendrites. Black and white small circles on the lines are excitatory and inhibitory synapses, respectively. (B) Place inputs from DG. (C) Theta input from MS. (D) Spike raster plot during trials. Colored plots are spikes of the excitatory units and black plots are that of the inhibitory unit. (E) Zoom up of (D) from 3 to 5 seconds. (F) The membrane potential of each neural unit. The X-axis and color of each unit correspond to (D).

The synaptic weights between neuronal units that received adjacent place inputs, were increased with the Hebbian plasticity and those of the other synapses in the same postsynaptic unit decreased with regularization plasticity. The synaptic weights in the forward order (from earlier to later activated units) were more potentiated than those in the reverse order (from later to earlier activated units) (Figure 2A and B). The time course of synaptic weight potentiation differed between the order directions (Figure 2C). These plastic changes in synaptic weights caused the accelerated timing of spikes in Figure 1D-F.

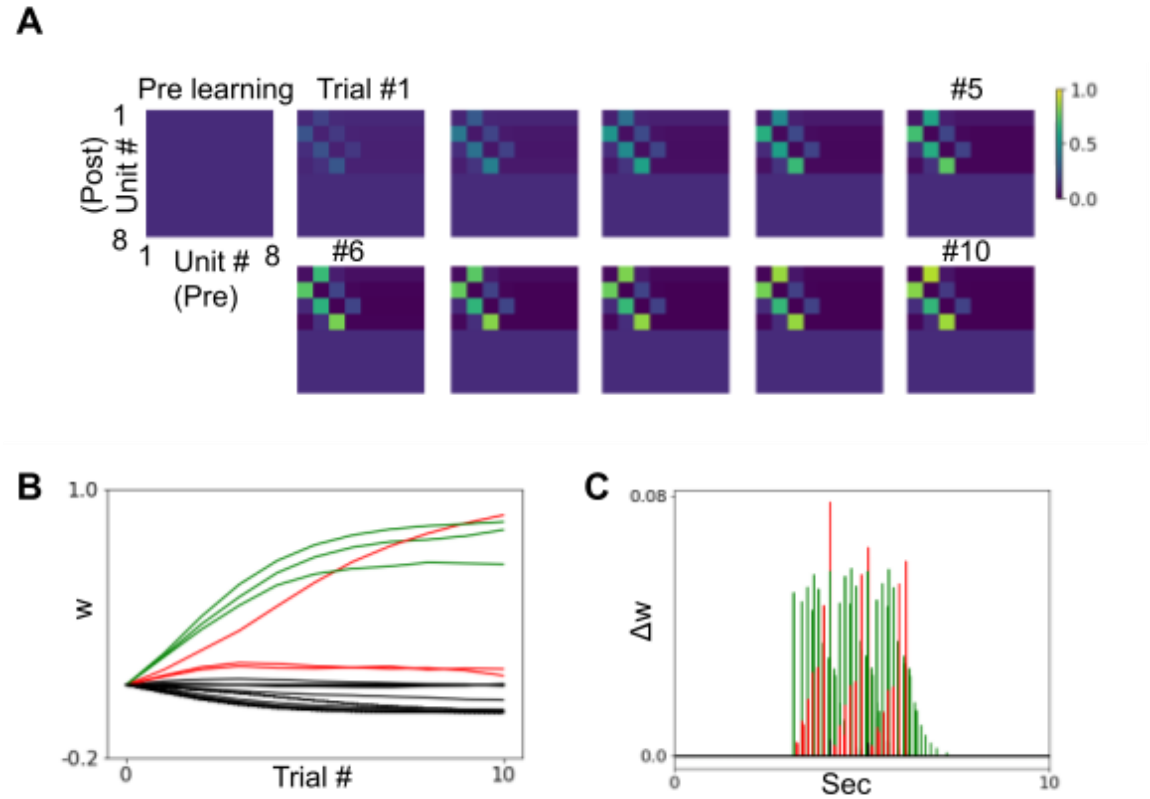

Figure 2 Synaptic weight change
(A) Synapse weight of CA3 excitatory-CA3 excitatory recurrent connection in each trial. (B) The synapse weight as a function of trial numbers. The green lines are synapses in forward order. Red lines are those in reverse order. Black lines are the other connections. (C) Synaptic weight changes (before regularization) during trial 1. The line color means the same as (B).

This model demonstrated theta oscillation as a population signal (Figure 3A and B) and theta phase precession-like firing pattern in the last trial (Figure 3D-F unit #2-4) except the unit receiving first place filed inputs (Figure 3D blue dots, Figure 3E and F unit #1). In contrast, the theta phase precession-like firing did not appear in the first trial (Figure 3C, E, and F). During the last trial, the excitatory units that received place inputs began firing at earlier positions than they did in the first trial, resulting in a negative slope of regression in unit #2-4 (Figure 3C-F; two-tailed paired t-test, n = 10; unit #1, p = 0.066, t = 2.092; unit #2, p = 0.005, t = -3.668; unit #3, p = 0.000, t = -17.443; unit #4, p = 0.002, t = -4.267; Figure 3F). The enhanced synaptic

weight of recurrent connections in Figure 2 caused these additional spikes. The model demonstrated the theta-precession pattern generation by learning the sequence.

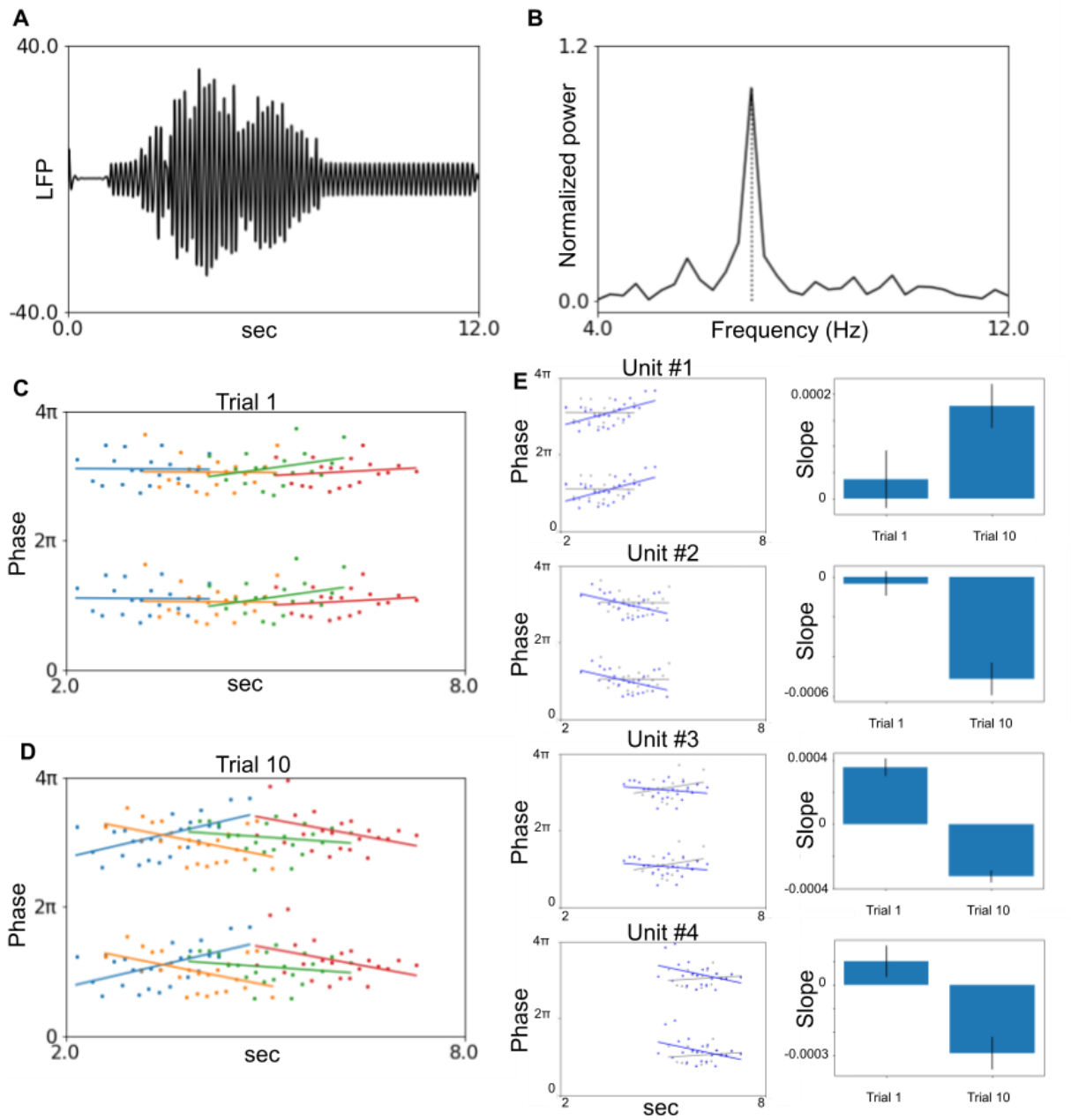

Figure 3 Phase precession
(A) LFP (local field potential: summation of membrane potentials of CA3 excitatory units) trace. (B) Frequency spectrogram of the LFP. (C) A plot of theta phase and time (corresponding to the position) in trial 1. The colors of the points correspond to Figure 1D-F. (D) Same plot as (C) in trial 10. (E) Spiking phase vs time plot in trial 1 (gray) and 10 (blue) of individual units are overlaid. (F) The regression coefficient of trial 1 and trial 10 in individual units. The order of panels is the same as (E).

Next, we tested whether the model could replay the sequential activity without external place inputs. To simulate a resting state of animals, we added a noisy input independently to each

neural unit, cutting off external place and theta inputs and shutting off plasticity in recurrent connections (resting session). After learning, the noise input occasionally induced random spikes, followed by sequential spikes of the associated units (Figure 4B). This did not appear before learning (Figure 4A). The lags between spikes among units, which received place inputs (responded units), were smaller than the other unit pairs after learning (Figure 4D) but not before learning (Figure 4C). By running multiple models, we confirmed the densities of spike pairs within 100 ms lag were significantly more among responded unit pairs (two-tailed paired t-test, $n = 10$, $p < 0.001$, $t = 18.493$, Figure 4E upper) but not among other types of pairs ($p = 0.394$, $t = -0.895$, Figure 4E middle; $p = 0.491$, $t = 0.718$, Figure 4E lower). The difference in peak positions of place inputs during learning and lags during replay after learning between responded units are significantly positively correlated in -200 to 200 ms lag (Figure 4F right, linear regression: $n = 104$, slope = 47.42, intercept = 4.43, $r = 0.44$, $p < 0.001$), indicating this model exhibited forward replay mainly. we excluded unit #1 from the regression analysis because it shows different patterns in theta phase precession from other units. This is also because of strengthening synaptic weights between neighbor place field units (Figure 2). The model successfully reproduced replay spike sequences after learning the place sequence.

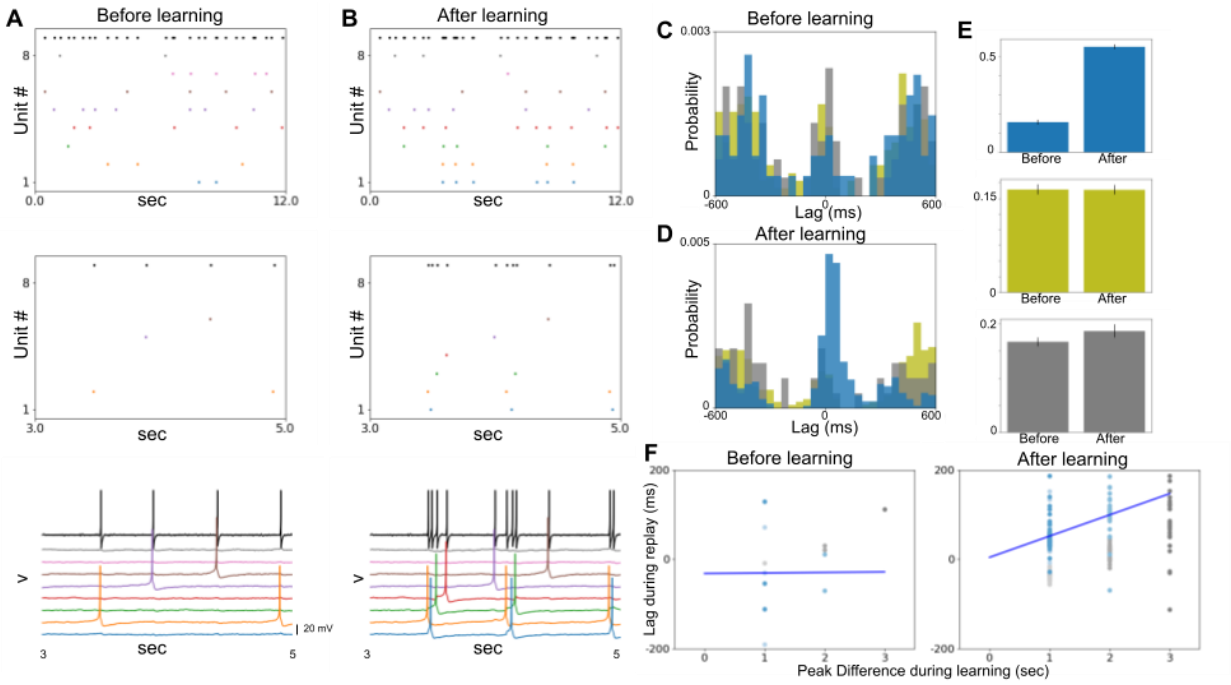

Figure 4 Replay

(A) Top: Spike plot in resting session with noise input before learning. The colored dot indicates the excitatory units and the black dot is the inhibitory unit. Middle: Zoom up on the upper panel for 2 seconds. Bottom: Membrane potentials of each neural unit. The x-axis and color of each unit correspond to the middle panel. (B) same as (A) in the resting session after learning. (C) Crosscorrelogram of CA3 excitatory units of resting session before learning. (D) Crosscorrelogram of the resting session after learning. Blue shows pairs among responded (they receive I_p) units during the running session. Yellow shows pairs between responded and non-responded units. Gray shows pairs among non-responded units. (E) the densities of spike pairs within 100 ms lag among responded unit pairs (upper), between responded and non-responded pairs (middle), and among non-responded pairs (lower). (F) Scatter plot of the difference in peak positions of place inputs during learning and lags during replay before (left) and after (right)

learning between responded units. The blue points show pairs excluding unit #1 and the gray points show those including unit #1. The blue lines show the results of the linear regression of the blue points.

We tested models by partially altering the elements of the original model (see Materials and Methods). A model with self-connection showed theta phase precession but not the sequential replay like in the original model (Figure 4—figure supplement 1). A model without coincident detection did not exhibit the theta phase precession and the replays (Figure 4—figure supplement 2). A model with a shorter time constant of plasticity-related factor also did not show theta phase precession and replays (Figure 4—figure supplement 3). A model without the theta input from MS displayed the replay but not the theta phase precession (Figure 4—figure supplement 4). The weakening synaptic weight caused the deficits of the model without coincident detection and the model with a shorter plasticity-related factor time constant. By increasing learning late (ten times larger) the models recovered the replay in forward or reverse order (Lower panels in Figure 4—figure supplement 2 and 3). The elements are necessary for efficient acquisition for the theta phase precession and the replay.

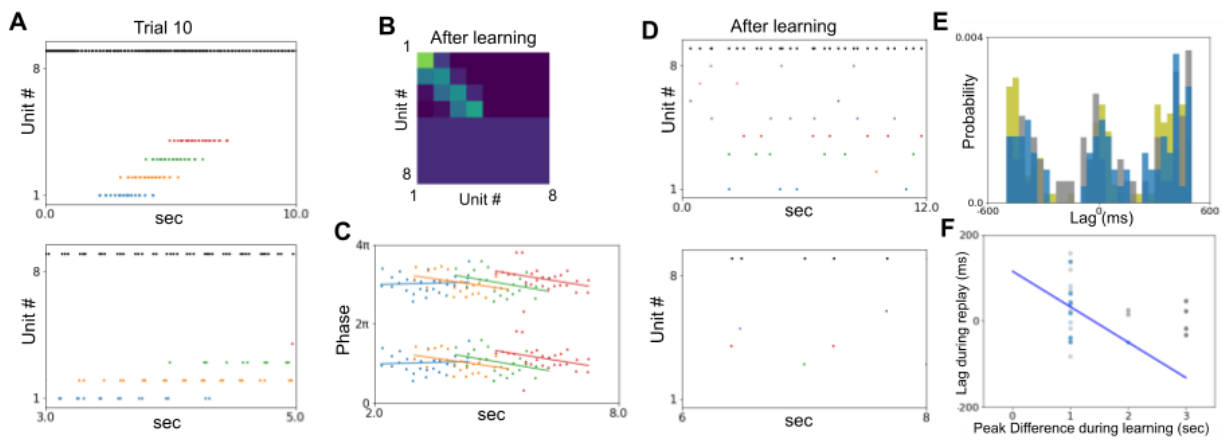

Figure 4—figure supplement 1 Small model with self-connection in the recurrent synapse
It exhibited the synaptic weights enhancement with neighbor units and theta phase precession, but not the replay. (A) Upper: Spike plot of trial 10. Bottom: zoom up from 3 to 5 seconds of the upper panel. (B) Synapse weights after learning. (C) Phase precession after learning. (D) Upper: spike activity in resting session with noise input after learning. Bottom: 2 seconds zoom up of the upper panel. (E) Crosscorrelogram of the resting session after learning. (F) Scatter plot of the difference in peak positions of place inputs during learning and lags during replay after learning between responded units. The colors and initial setting correspond to those in Figure 1-4.

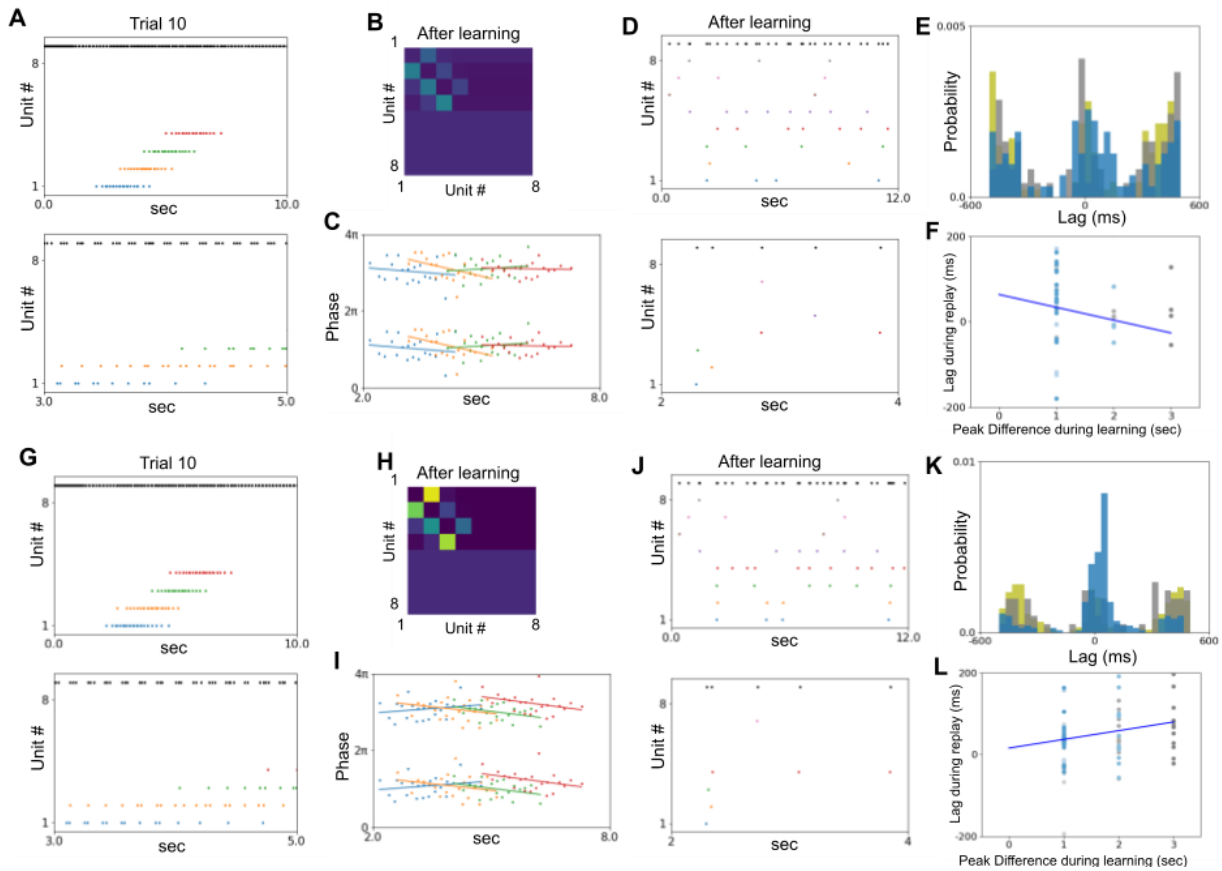

Figure 4—figure supplement 2 Small model without coincident detection

The synaptic weight enhancement was weakened. The theta phase precession and the replays were not observed, which were recovered with larger learning rate. (A) Upper: Spike plot of trial 10. Bottom: zoom up from 3 to 5 seconds of the upper panel. (B)Synapse weights after learning. (C) Phase precession after learning. (D) Upper: spiking activity in resting session with noise input after learning. Bottom: 2 seconds zoom up of the upper panel. (E) Crosscorrelogram of the resting session after learning. (F) Scatter plot of the difference in peak positions of place inputs during learning and lags during replay after learning between responded units. (G-L) same as the above panels with a ten times larger learning rate. The colors and initial setting correspond to those in Figure 1-4.

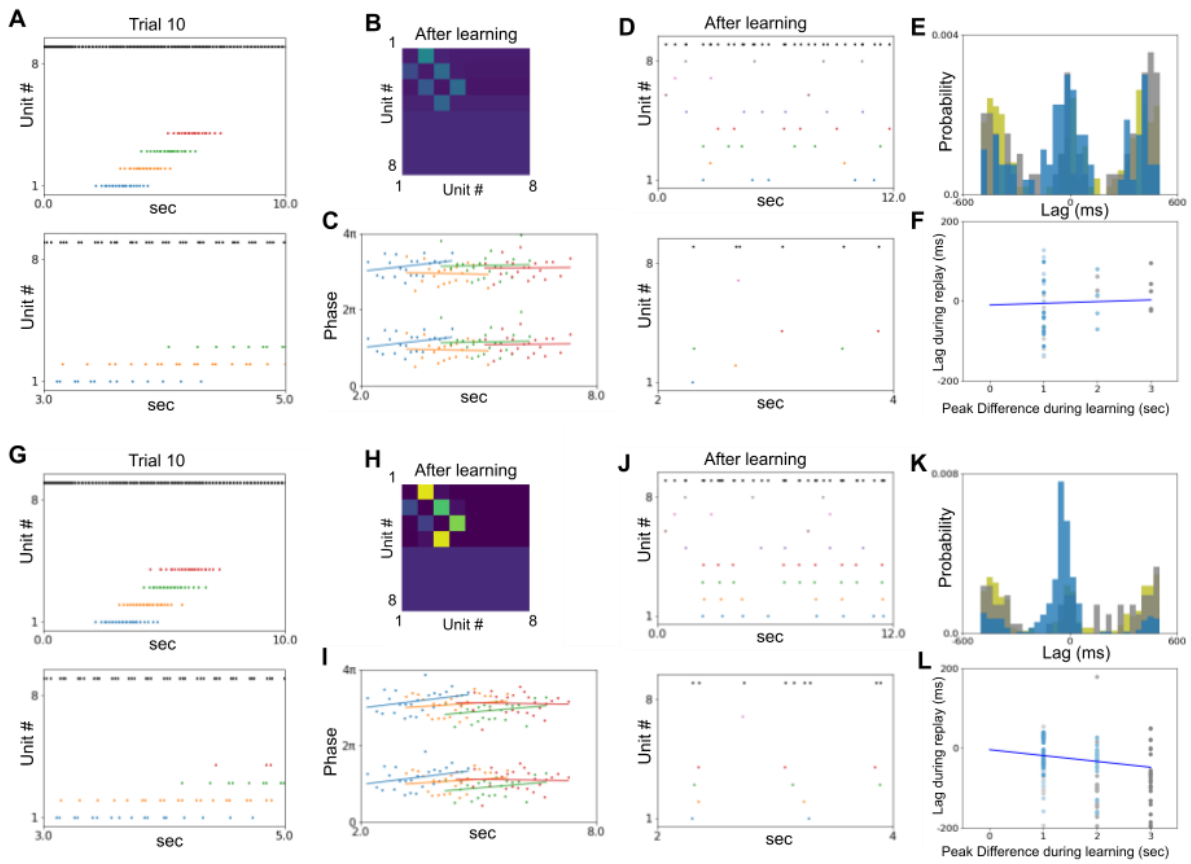

Figure 4—figure supplement 3 Small model with shorter time constant of plasticity-related factor
The synaptic weight enhancement was weakened. The theta phase precession and the replays were not observed, which were recovered with larger learning rate while the order was reversed. (A) Upper: Spike plot of trial 10. Bottom: zoom up from 3 to 5 seconds of the upper panel. (B) Synapse weights after learning. (C) Phase precession after learning. (D) Upper: spiking activity in resting session with noise input after learning. Bottom: 2 seconds zoom up of the upper panel. (E) Crosscorrelogram of the resting session after learning. (F) Scatter plot of the difference in peak positions of place inputs during learning and lags during replay after learning between responded units. (G-L) same as the above panels with a ten times larger learning rate. The colors and initial setting correspond to those in Figure 1-4.

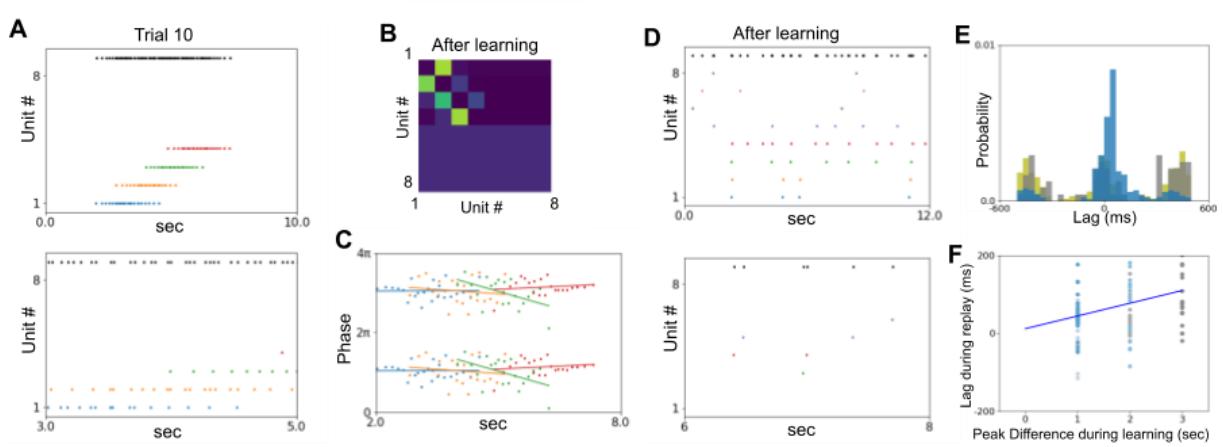

Figure 4—figure supplement 4 Small model without theta input from MS

The theta phase precession was not observed, but the synaptic weight enhancement with neighboring units and the relay was still observed. (A) Upper: Spike plot of trial 10. Bottom: zoom up from 3 to 5 seconds of the upper panel. (B) Synapse weights after learning. (C) Phase precession after learning. (D) Upper: spiking activity in resting session with noise input after learning. Bottom: 2 seconds zoom up of the upper panel. (E) Crosscorrelogram of the resting session after learning. (F) Scatter plot of the difference in peak positions of place inputs during learning and lags during replay after learning between responded units. The colors and initial setting correspond to those in Figure 1-4.

We tested the ability of the model to learn an additional sequence (the order of unit #4-5-6-7, Figure 5A) following the initial sequence learning (Figure 1-4). The first DG input of the new sequence was the same as the last one of the initial sequence set (unit #4, Figure 1B red line), while the other DG inputs differed from those in the initial sequence set. Like the initial sequence learning, the model demonstrated a shift in spike timing across trials in the additional learning stage (Figure 5B). The weights of the pairs within the additional sequence were strengthened, while the weight strengths of the pairs within the initial sequence were maintained to some extent (Figure 5C). Additionally, the model exhibited theta phase precession in the units that had learned the additional sequence (Figure 5D). During the resting session, the model displayed replay-like activity of the additional sequences set mainly in forward order (slope=54.2, intercept=-10.7, r=0.43, p<0.001, n=122), and also the initial sequence set while it lost the direction of the order (slope=-36.8, intercept=70.3, r=-0.26, p=0.11, n=40) (Figure 5E-G). These results suggest that the model can learn additional sequences while retaining the associative information of the initial sequence.

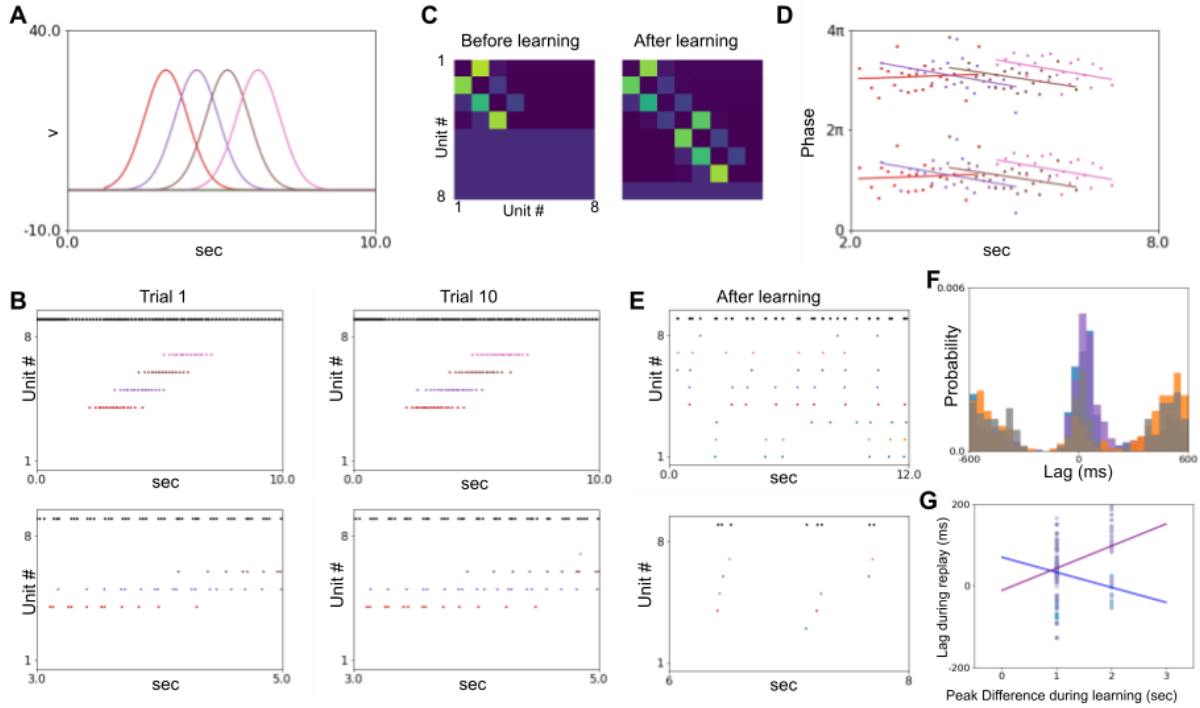

Figure 5 Additional learning
(A) Place inputs from DG. (B) Upper: spike plot of trial 1 and 10. Bottom: zoom up from 3 to 5 seconds of the upper panels. The colored dots show the excitatory spikes, and the black dots show inhibitory spikes. The colors correspond to those in Figure 1-4. (C) Synapse weights before (left) and after (right) the additional learning. (D) Phase precession after learning. (E) Spike plot of replay in resting session with noise input after learning. The lower panel is zoomed up on the upper panel for 2 seconds. (F) Crosscorrelogram of the resting session after learning.

Purple shows pairs of additional sequence. Blue shows pairs of the initial sequence (Figure 1-4). Orange shows pairs between the initial and the additional sequence. Gray shows the other pairs. (G) Scatter plot of the difference in peak positions of place inputs during learning and lags during replay after the additional learning. The purple points show pairs of the additional sequence (excluding unit #4) and the blue points show pairs of the first sequence (excluding unit #1). The purple and blue lines show the linear regression results of each colored point.

The ability of the model to relearn the new sequence which was a mixture of the previous and new place fields was also examined (the order of unit #8-1-3-6, Figure 6A) after the initial sequence learning (Figure 1-4). The second and third-place inputs in the relearning sequence set were the same as the first (unit #1) and third (unit #3)-place inputs in the initial sequence set. During the earlier trial, the units of the initial sequence set were spiked (yellow and red dots in Figure 6B left), but these activities disappeared following relearning (Figure 6B right). The synaptic weights underwent a reorganization to accommodate the new relearning sequence (Figure 6C). The connections between the initial sequence set remained, although the synaptic weights were somewhat weakened. The theta phase precession of the relearning sequence was observed (Figure 6D). During the resting session, the model showed replay-like activity of the relearning sequence set in forward order (slope=72.1, intercept=-27.6, r=0.63, p<0.001, n=80), and also those of the initial sequence set with losing the direction of the order (slope=22.1, intercept=-0.54, r=0.17, p=0.114, n=86) (Figure 6E-G).These results indicate that the model can adaptively reorganize new sequence sets.

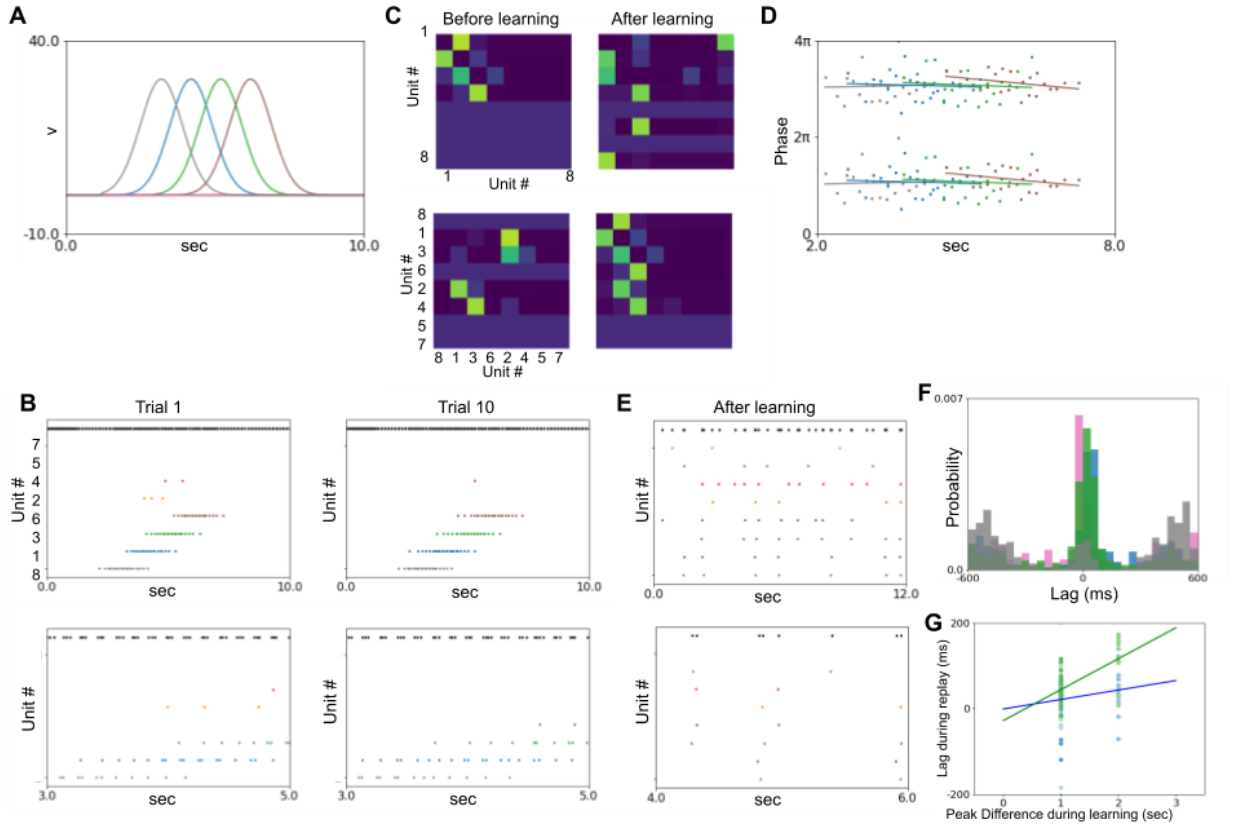

Figure 6 Relearning

(A) Place inputs from DG. (B) Upper: spike plot of trial 1 and 10. Bottom: zoom up from 3 to 5 seconds of the upper panels. The colored dots show the excitatory spikes, and the black dots show inhibitory spikes. The colors correspond to those in Figure 1-4. (C) Synapse weights before (left) and after (right) the relearning. The upper panels are in the original order, and the lower panels are in the order of responded units in the relearning. (D) Phase precession after relearning. (E) Spike plot of replay in resting session with noise input after learning. (F) Crosscorrelogram of the resting session after relearning. Green shows pairs of relearning sequence. Blue shows pairs of the initial sequence (Figure 1-4). Magenta shows pairs between the initial and the relearning sequences. Gray shows the other pairs. (G) Scatter plot of the difference in peak positions of place inputs during learning and lags during replay after the relearning. The green points show pairs of the relearning sequence (excluding unit #8) and the blue points show pairs of the initial learning sequence (excluding unit #1). The green and blue lines show the linear regression results of each colored point.

In the above study, we tested the minimal network model and determined synaptic connections. In the real CA3 circuit, many more neurons and the synaptic connections are probabilistic. To replicate this in a more realistic simulation, we constructed a larger model using the Brian2 simulator (Stimberg et al., 2019). Like the small network, this model received two types of external input: the place input from DG to the CA3 excitatory units (Figure 7A) and theta inhibitory input from MS to the CA3 inhibitory units (Figure 7B). A tiny population of CA3 excitatory units was connected with and spiked by the DG place inputs (the probability of the DG-CA3 excitatory connection $p_{pe} = 0.005$), while all CA3 inhibitory units showed theta-locked burst spikes (Figure 7C). The CA3-CA3 recurrent synaptic connections were also probabilistic (the probability of the recurrent connection $p_{rec} = 0.1$) but much denser than DG-CA3 synapses, and plasticity was implemented using the Hebbian rule. we selected the responded excitatory units (referred responded units) to observe the formation of the sequential activity (Figure 7D). A portion of the units exhibited an earlier onset of activity during the last trial as a result of the learning (Figure 7E), and some synaptic weights between the responded units were enhanced (Figure 7F). Theta phase precession was also observed in the units following learning (Figure 7G and 7H). The model demonstrated replay activity during the resting session (Figure 7J-7L). The large network model produced results consistent with those of the small network model.

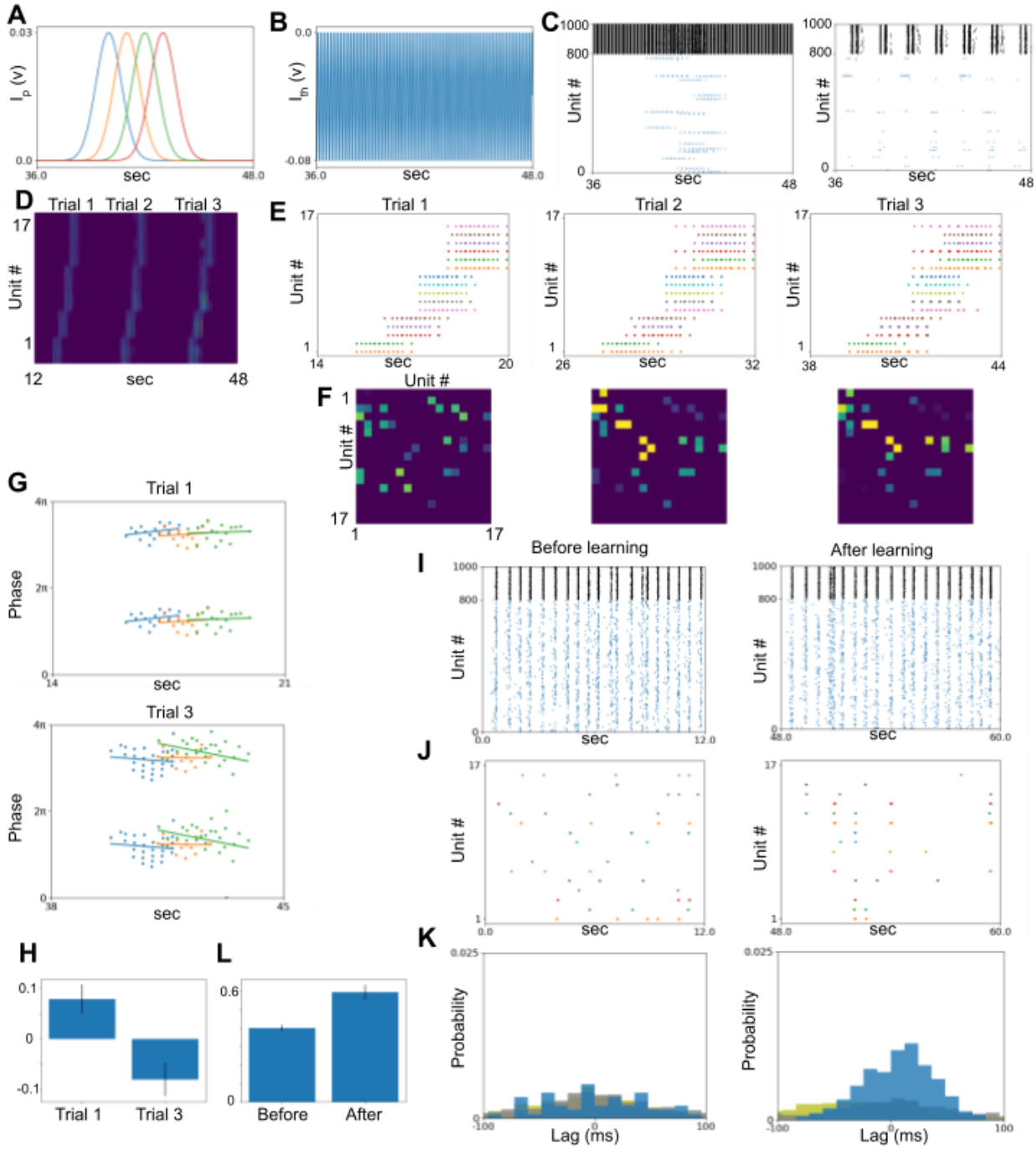

Figure 7 Large-scale network

(A) Place input from DG. (B) Theta input from MS. (C) Spike raster plot of excitatory (blue) and inhibitory (black) units. (D) The color plot of the spike rate of excitatory units responded to place inputs. They are sorted by peak response position and concatenated from trial 1 to 3. (E) Spike raster plots of the responded units from trial 1 (left) to 3 (right). Note that the first spikes of some units proceeded in later trials. (F) Synaptic weights between the responded units from trial 1 (left) to 3 (right). (G) theta phase precession in trial 1 (upper) and 3 (lower). (H) The regression coefficient of responded units in trial 1 and 3 with multiple models (Paired t-Test, n = 57, t = -3.535, p = 0.001). (I) Spike raster plot of all units in resting session with noise input before (left) and after (right) learning. The color is the same as in Figure 7C. (J) Spike raster plot during the resting session of responded excitatory units. (K) Crosscorrelogram in the resting session. Blue shows unit pairs between responded units. Yellow shows unit pairs between responded and

non-responded units. Gray shows unit pairs between non-responded units. (L) the densities of spike pairs within 100 ms lag among responded unit pairs before and after learning with multiple models (Paired t-Test, n = 15, t = 4.283, p = 0.001).

Next, we analyzed the dynamics of each type of unit when the external inputs (I_p^{exc}, I_{th}^{inh}) were supplied. The parameters of the excitatory and inhibitory neural units of the above models were referred to (Izhikevich, 2010). The dynamics of the Izhikevich model can be depicted as a phase portrait in the v-u coordinate plane, which helps visualize the behavior of the model over time. (Figure 8A and 8B). Non-linear neural models, such as the Izhikevich model, exhibit bifurcations (Figure 8C and 8D). These bifurcation points are crucial for describing the activity of the neural model. The excitatory neural units had a stable point when there was no external input (Figure 8A black circle). A stable point indicates that the neuron remains in a steady state, not generating action potentials. If the external input *I* exceeds the bifurcation point *I* = 24.5 (Figure 8C) with place DG input, the stable point was lost, and bursting occurred (saddle-node bifurcation). When the external input decreased, the stable point reappeared, and the firing became silent. When the inhibitory input was provided from the CA3 inhibitory unit, the quadric v-nullcline moved in minus direction on the u-axis, causing a delay in firing (if the stable point did not appear) or stopping the firing altogether (if the stable point had appeared). These dynamics are the behavior of excitatory units in the simulated scenarios described above.

In the absence of MS theta inhibitory input (baseline, *I* = 100), the inhibitory neural unit had an unstable point and exhibited bursting firing (Figure 8B solid line and white circle). When the inhibitory theta input received from MS and the external input falls below *I* = 73.7, the unstable point becomes stable (Andronov-Hopf bifurcation, Figure 8B dash line and black circle). When the point was stable, the dynamics of the unit converged on it and stopped firing. However, decreasing the amplitude of the theta inhibitory input caused the stable point to become unstable again, resulting in the reemergence of burst firing.

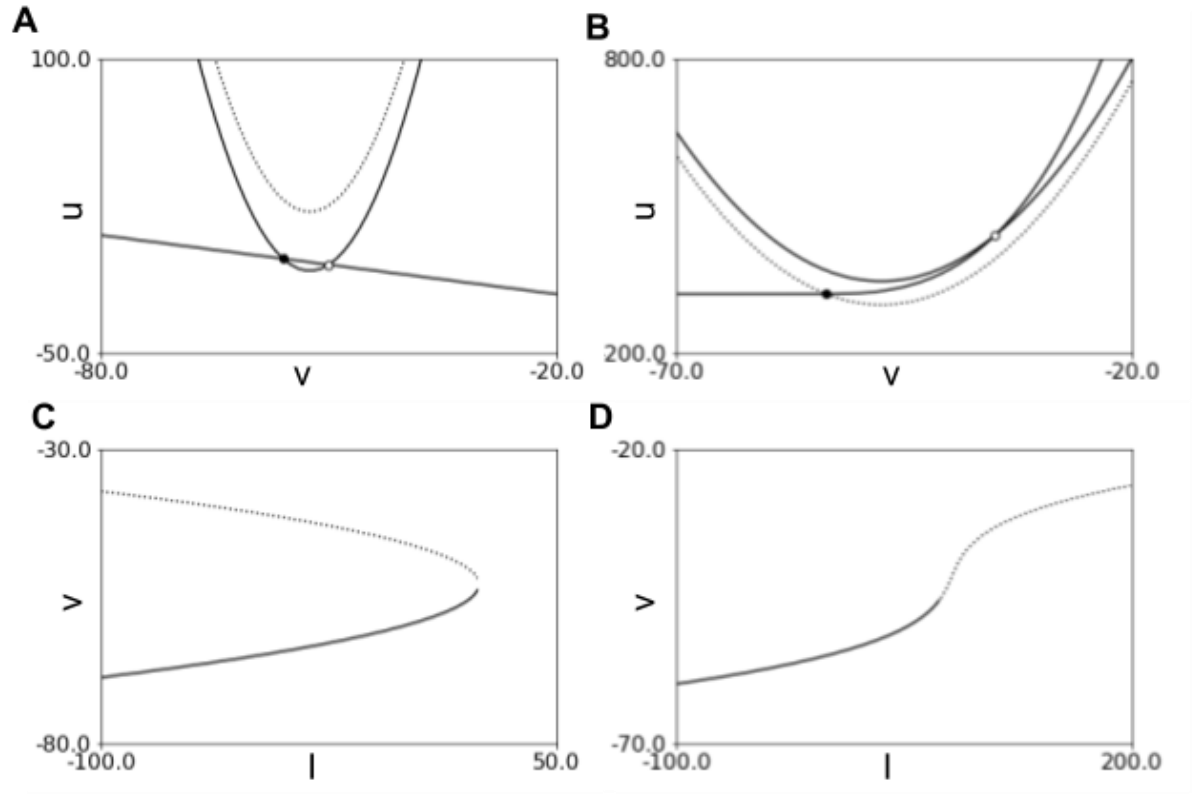

Figure 8 Bifurcation properties of excitatory and inhibitory units
(A) Phase portrait of the excitatory unit. The quadratic curve is the v-nullcline and the straight line is the u-nullcline. The solid line indicates a v-nullcline without external input. The dotted line indicates v-nullcline with maximum I_p. The black and white circles indicate stable and unstable equilibrium, respectively. (B) Phase portrait of the inhibitory unit. The dotted line indicates v-nullcline with minimum I_{th}. (C) Bifurcation diagram depending on external input *I* of the excitatory unit. The solid and dotted lines indicate stable and unstable equilibrium, respectively. (D) Bifurcation diagram depending on external input *I* of the inhibitory unit.

The amplitude of the external input affected the spike timing of the excitatory units in the theta cycle (Figure 9A-D). The MS inhibitory input controlled the theta cycle (Figure 9A). As described above, the CA3 excitatory unit does not spike without the external DG place input (Figure 8A solid line and Figure 9C c). When the external input amplitude increased slightly above the bifurcation point, the units began firing later in the theta cycle (Figure 9C a). With a small amplitude of external input, the transition speed around the closest area between v- and u-nullclines is very slow (Figure 9C a lower). As the external input amplitude increased, the equilibrium disappeared, the transition speed around the area became faster, the firing timing in the theta cycle became earlier, and the unit began to burst (Figure 9C b). The firings were restricted and reset by inhibitory inputs from the CA3 inhibitory unit, which spiked at specific phases in the theta cycle (Figure 9D). This resetting by the inhibitory input caused the start timings of the state in the v-u coordinate of each excitatory unit to be aligned with the theta cycle.

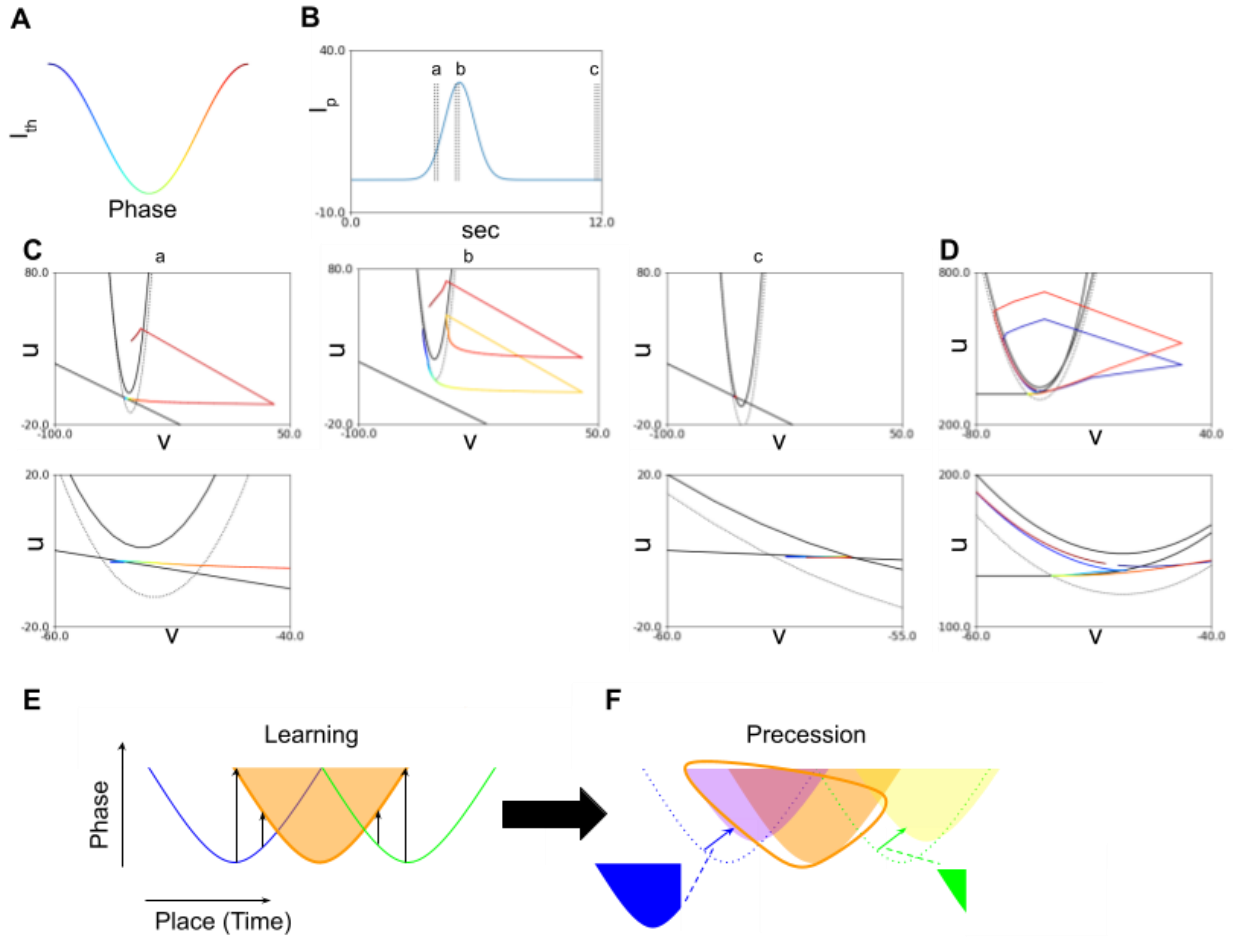

Figure 9 Firing timing in the theta cycle phase with place inputs
(A) Correspondence between one cycle of theta oscillation and color in I_{th}. (B) Single place input I_p. Characters a, b, and c correspond to the one theta cycles plotted in (C). (C) The upper panels are the trajectory of the excitatory unit in the v-u phase portrait at the theta cycle of a, b, and c, respectively, in (B). Colors correspond to the colors of the theta cycle in (A). Lower panels are expansions of the upper panels around the closest or cross area between the v- and u-nullcline. (D) The upper panel is the trajectory of the inhibitory unit without place input I_p, corresponding to c in (B). The lower panel expands the upper panel around the closest area between the v- and u-nullcline. (E and F) Schematic illustration of the acquisition process of phase precession and replay in this model. (E) Before learning, the firing timings of a neuronal unit (orange shadow and line) on the phase-place (time) plane depend on place input strength, displaying a symmetric shape. Synaptic potentiation occurs (black arrow) with the CA3 excitatory unit responding to the anterior (blue line) and posterior (green line) place inputs. (F) The synaptic potentiation takes effect slightly later (colored arrows) than the firing of the previous neural unit (purple and yellow shadows), either accelerating the spike timing or inducing spikes in an additional theta cycle. The difference in plasticity-related factor accumulation (blue and green opaque shadows) and the overlapping area between the anterior (purple shadow) or posterior (yellow shadow) units and the center unit (orange shadow) results in a stronger effect from the anterior responding unit, leading to an asymmetric precession shape (orange line). The synaptic potentiation also affects replay.

Following the explanation, the phase precession pattern should be symmetric (no bias in the phase position of spikes before and after the peak position), as it depends solely on place input

strength, which is symmetric in this model. Additional synaptic interactions shape the negative slope precession pattern. Before learning, the phase precession pattern of a CA3 excitatory neuronal unit is symmetric (Figure 3C and Figure 9E orange shadow; referred to as the center unit). The learning process enhances recurrent synaptic weights, connecting units responding to anterior and posterior place inputs (Figure 9E blue and green lines; referred to as anterior and posterior units, respectively) (Figure 2A). The difference in firing timing with the anterior and posterior units is also symmetric (Figure 9E arrows). The synaptic potentiation increases input amplitude and advances spike timing in the postsynaptic units (center unit) while also causing spikes in the late phase of the earlier theta cycle. The effect of synaptic input occurs slightly later than the presynaptic (anterior and posterior units) spike timings, creating an asymmetric effect where the anterior unit has more time to overlap with the activated timing of the center unit than the posterior unit (Figure 9F purple-orange and yellow-orange shadow overlapping areas, respectively). Furthermore, the anterior unit interacts with the center unit during the latter part of its activity whilehe posterior unit interacts during the earlier part. This causes the plasticity-related factor (see Materials and Methods) to accumulate more in the anterior unit, resulting in greater synaptic potentiation than in the posterior unit (Figure 2C and Figure 9F blue and green opaque shadows, respectively). These mechanisms lead to an asymmetric phase precession pattern. Additionally, the strengthened synapses induce sequential spikes by noisy random input in the resting session. In our models, this mechanism establishes theta phase precession and replays after place learning.

Discussion

In this study, we developed a neural circuit model based on anatomical evidence of the biological CA3 circuits. The model was able to learn and compress the order of external inputs from sparse DG projections using the Hebb rule and displayed theta phase precession and replay-like activity. The model was also able to perform additional learning and relearning. These results suggest that the characteristic hippocampal activity of learning sequential events, theta phase precession, and replay in SWR are mediated by plastic changes in the synapses of the CA3 recurrent circuit.

The region responsible for the encoding sequence is still debated (Drieu and Zugaro, 2019). In this research, we assumed that the CA3 recurrent connection plays a role in sequence learning based on anatomical (the CA3 has a relatively dense recurrent connection) and electrophysiological (source of SWR) evidence (Buzsáki, 2015; Hájos et al., 2013; Rebola et al., 2017; Schlingloff et al., 2014). Most of the replay in SWR has been reported in the CA1 (Johnson and Redish, 2007; Karlsson and Frank, 2009). CA3 is likely the source of replay, as input from the CA3 has been observed when the CA1 ripple occurs (Buzsáki, 2015; Csicsvari et al., 2000) and the replay collapses when CA3 is lesioned (Middleton and McHugh, 2016). The CA3 lesion also affects CA1 replay (Davoudi and Foster, 2019; Guan et al., 2021; Yamamoto and Tonegawa, 2017). There are also reports of theta phase precession (Dragoi and Buzsáki, 2006; Fernández-Ruiz et al., 2017; Mizuseki et al., 2012; Oliva et al., 2016; Sharif et al., 2021) and replay (Carr et al., 2012; Diba and Buzsáki, 2007; Hwaun and Colgin, 2019; Karlsson and

Frank, 2009; O'Neill et al., 2008) in the CA3. The CA3-CA1 connection can also learn sequences, like reservoir networks (Cazin et al., 2019; Enel et al., 2016). The DG-CA3 giant synapses are still a potential candidate for the region responsible for sequence learning. In this study, we excluded inputs from the entorhinal cortex, which have been shown to affect theta phase precession (Fernández-Ruiz et al., 2017; Schlesiger et al., 2015) and replay (Chenani et al., 2019; Yamamoto and Tonegawa, 2017) in the hippocampus. To fully understand the main region responsible for sequence learning, it will be important to integrate these experimental findings and computational frameworks in the future.

Models that explain theta phase precession can be divided into three main categories (Drieu and Zugaro, 2019): detuned oscillator models (Geisler et al., 2010; O'Keefe and Recce, 1993), somato-dendritic interference models (Harris et al., 2002; Kamondi et al., 1998; Mehta et al., 2002), and network connectivity models (Jensen and Lisman, 1996; Romani and Tsodyks, 2015; Skaggs et al., 1996; Tsodyks et al., 1996). The detuned oscillators model posits that phase precession arises from single place cell oscillating at a slightly faster frequency than the population signal (LFP) theta oscillation, with both oscillators gradually shifting due to their frequency difference. Our findings do not support this model, as the LFP (summation of all excitatory membrane potential) and the individual neuronal firing or membrane potential frequency in our model were identical (Figure 3B). In contrast, somato-dendritic interference models suggest that a combination of oscillatory somatic inhibition and transient ramp-like dendritic excitation determines action potential timing. Our results support this model, as place input strength dictates spike timing in space in the absence of recurrent inputs (Figure 8 and 9). Furthermore, the expansion of the place fields (Figure 1D-F) also supports the development of the precession with the somato-dendritic interference model (Mehta et al., 2002, 2000). Network connectivity models propose that phase precession results from transmission delays between asymmetrically connected cells. Our results align with this model, as our model exhibits additional spikes in the late phase of the early theta cycle after learning (Figure 1-3). These findings highlight the potential roles of somato-dendritic interference and network connectivity in phase precession, although our model does not exhaustively explore these mechanisms.

In our model, phase precession gradually forms through learning, consistent with Mehta et al. (2002). However, it does not align with Feng et al. (2015), which reported that phase precession of individual place cells was present from the initial trial and became more aligned across cells as the number of trials increased, forming theta sequences. In this study, our model assumed nearly uniform membrane properties and synaptic connections in its initial state. By introducing variabilities in these values, such as distinct cellular properties and prewired connections for each cell, it might be possible to reproduce the results of Feng et al. within our model. Another possibility is that the difference arises from the distinct characteristics of CA3 and CA1, as these reports focus on CA1.

There is a debate regarding the replay, whether it is pre-existing (Dragoi and Tonegawa, 2011) or acquired (Silva et al., 2015). Many computational mechanisms for achieving replay sequences have been proposed in computational modeling studies (August and Levy, 1999; Ecker et al., 2022; Haga and Fukai, 2018; Jahnke et al., 2015; Jensen et al., 1996; Nicola and

Clopath, 2019; Reifenstein et al., 2021). The results of this study explained how a recurrent network could acquire the replay sequences, incorporating both pre-existing and acquired aspects. Specifically, task-related and strongly connected synapses before learning tend to be enhanced through repeated experience.

In our model, primarily forward replay was observed. However, it may be possible to reveal different patterns, such as reverse replay, by altering synaptic learning rules (for example, our model used an asymmetric Hebbian rule, but other options could include standard STDP (Bi and Poo, 1998) or symmetric STDP (Mishra et al., 2016)) or by imposing an upper limit on synaptic strength.

Models similar to our model include Jensen et al. (Jensen et al., 1996; Jensen and Lisman, 1996) and Ecker et al. (Ecker et al., 2022). Both our and these other models learned the order in which place cells are active in the CA3 recurrent connection through the Hebb rule or similar learning rules (symmetric STDP) (Mishra et al., 2016). As a result of learning, all models showed a non-Gaussian, asymmetric distribution of synapse weights. Experimental results in biological brains also suggest the occurrence of similar phenomena (Choi et al., 2018). However, several distinctive features of our model set it apart; (1) In contrast to the other models, our model includes theta input as inhibitory input to inhibitory units. This is supported by optogenetic experiments showing that theta rhythm input is mediated by inhibitory projections from MS to PV-positive inhibitory neurons in the hippocampus (Zutshi et al., 2018). (2) Our model also reproduces the decrease in inhibitory neuron activity during sleep or rest (Haider et al., 2013; Miyawaki and Diba, 2016), which leads to an increase in random firing and the potential induction of replay during resting sessions. (3) While Jensen et al. focus on phase precession (with no mention of replay) and Ecker et al. demonstrate the occurrence of SWR-like activity and accompanying forward and reverse replay (with no mention of precession), our model aims to reproduce both the characteristic precession and replay activity in the hippocampus through learning in the CA3 local circuit and recurrent connection. These unique aspects of our model provide new insights and a more comprehensive understanding of the CA3 circuit's role in theta phase precession and replay activity in the hippocampus.

This study has proposed a mechanism for compressing the sequence of external events into theta phase precession and replay. However, several points still need to be revealed. First, is the formation of precession and replay pre-existing or acquired? we believe both aspects exist; the pre-existing circuits existed before learning and are reinforced by learning. Additionally, An interesting area of examination would be how the neuronal synchronization state of the hippocampus changes during activity, sleep, and rest, and how replay occurs; whether replay in the CA3 has different functions than replay in the CA1 and other brain regions; whether synaptic plasticity is activated during replay; the contribution of circuits other than CA3; and the effects of learning on replay. Further research is needed to investigate these questions from experimental and computational approaches.

Replay in the HPC during sleep or rest may be related to memory consolidation, abstraction, planning, and inference (Buzsáki, 2015; Drieu and Zugaro, 2019). To perform these functions,

the replayed sequences should be variable in each replay, evaluated for some purpose, and interact with cortical networks. Therefore, it is essential to investigate these mechanisms in the near future.

Methods

Small Model

The CA3 model consisted of 8 excitatory and one inhibitory unit (Figure 1A). The excitatory units received the DG place inputs, recurrent CA3 connections, and inhibitory inputs from the CA3 inhibitory unit. The inhibitory unit received the theta MS inhibitory input and excitatory inputs from the CA3 excitatory units. The activity of the units was modeled using the Izhikevich model (Izhikevich, 2010) and the parameters were chosen according to Chap. 8.4.1 (Hippocampal CA1 Pyramidal Neurons) and Chap.8.2.6 (Fast Spiking Interneurons) for the excitatory and inhibitory units, respectively.

The Izhikevich model is described as follows:

$$C\frac{dv}{dt} = k(v - v_r)(v - v_t) - u + I \quad \text{(eq1)}$$

$$\frac{du}{dt} = a\{b(v - v_r) - u\} \quad \text{(eq2)}$$

, where v is the fast membrane potential, u is the slow recovery variable that allows for the replication of various neural cell types, v_r is the resting potential, v_t is the threshold potential for spike initiation, C is the membrane capacitance, a is the recovery time constant of u, k and b are scaling coefficients, I is the input to the neural unit, v_{peak} is the peak potential if v exceed v_{peak} the v and u are reset to $v \leftarrow c$ and $u \leftarrow u + d$, respectively. In the inhibitory unit,

$$du/dt = a^{inh}(B(v) - u)$$

$B(v) = 0$ when $v < v_r^{inh}$ and $B(v) = b(v - v_r^{inh})^3$ when $v \geq v_r^{inh}$ (eq3)

(Chap.8.2.6, (Izhikevich, 2010).

The CA3 excitatory unit received from excitatory DG place inputs, recurrent CA3 connections, and inhibitory inputs from the CA3 inhibitory unit.

$$I^{exc} = I_p^{exc} + I_{rec}^{exc} + I_{ie}^{exc} + I_{base}^{exc} + I_{noise}^{exc}$$

, where I_p^{exc} is the place input from the DG, I_{rec}^{exc} is the recurrent input from the CA3 excitatory units, I_{ie}^{exc} is the input from CA3 inhibitory unit to CA3 excitatory unit, I_{base}^{exc} is a constant baseline input, and I_{noise}^{exc} is a Gaussian noise input with $N\ (0, \sigma_{noise}^2)$. Similarly, the CA3 inhibitory unit received excitatory inputs from CA3 excitatory units and inhibitory theta input from MS.

$$I^{inh} = I_{th}^{inh} + I_{ei}^{inh} + I_{base}^{inh} + I_{noise}^{inh}$$

, where I_{th}^{inh} is the theta input from MS, I_{ei}^{inh} is input from the CA3 excitatory units, I_{base}^{inh} is a constant baseline input, and I_{noise}^{inh} is a Gaussian noise input. In the simulation, the σ_{noise} is scaled by the square of the time step ($\sigma_{noise}\sqrt{dt}$).

The synaptic inputs I_{syn} (I_{rec}^{exc}, I_{ie}^{exc}, I_{ei}^{inh}) of the unit i were described as follows:

$$I_{syn} = \sum_j g_{ij}(t) \cdot (E - v_i(t))$$

$$dg_{ij}(t) = -g_{ij}(t-1)/\tau + w_{ij}s_j(t)$$

, where $g_{ij}(t)$ is a synaptic conductance between presynapse j and postsynapse i, E is an equilibrium potential ($E_{ampa} = 0$ for excitatory synapses and $E_{gaba} = -65$ for inhibitory synapses), τ is a time decay constant of the synaptic conductance ($\tau_{ampa} = 10$ ms, $\tau_{gaba} = 20$ ms), $s_j(t)$ is a spike (0 or 1) of the presynaptic neural unit, and w_{ij} is a synaptic weight between pre and postsynaptic neural units. Note that I_{rec}^{exc} and I_{ei}^{inh} represent excitatory synapses (AMPA) and I_{ie}^{exc} represents inhibitory synapses (GABA-A).

The DG-CA3 excitatory unit connection (place input) was assumed to be sparse, meaning that each CA3 excitatory unit received only one place input. The amplitude of the place inputs was set high enough to induce spikes in the CA3 excitatory units with only one place input. This model used four place inputs for each session in 8 DG inputs. The CA3-CA3 recurrent connections were all-to-all and plastic (see section Plasticity section). All CA3 excitatory units sent spikes to the CA3 inhibitory unit, which in turn sent feedback inhibition to all CA3 excitatory units.

External Inputs

In this model, we assumed that the place inputs were from DG to CA3 excitatory neural units, and the theta inputs were from MS to CA3 inhibitory units.

The place inputs from DG were modeled as follows:

$$I_p^{exp} = a_p \cdot exp\{-(x(t) - x_{peak})^2/\sigma_p\}$$

, where a_p is the amplitude of the place input, $x(t)$ is the current position of the agent, x_{peak} is the peak position of the place field, and the σ_p is the width of the place field. Since the speed of the agent is assumed to be constant in this simulation, then $x(t) = t$ cm (velocity is 1 cm/s). The orders of inputs were as follows: initial learning, unit #1-2-3-4; additional learning, unit #4-5-6-7; relearning, unit #8-1-3-6.

The theta oscillation inputs from MS were modeled as follows:

$$I_{th}^{inh} = a_{th} \cdot \{sin(2\pi t/f_{th})/2 + 1/2\}$$

, where a_{th} is the amplitude of the theta input and f_{th} is the frequency of the theta oscillation. As the speed of the agent is assumed to be constant in this simulation, then f_{th} is also constant.

Plasticity

The synaptic weights of the CA3-CA3 recurrent connection were plastically changed according to Hebbian and regularization rules. The Hebbian plasticity between postsynapse unit i and presynapse unit j was modeled as

$$dw_{ij}^{rec} = a_{Hebb} \cdot s_i(t) \cdot g_{ij}^{l}(t)$$

$$dg_{ij}^{l}(t) = -g_{ij}^{l}(t-1)/\tau_l + s_j(t) I_{p,i}^{exc}(t)$$

, where a_{Hebb} is a learning rate of the Hebbian learning, s_i and s_j are spikes of postsynaptic and presynaptic neural units, respectively, and $g_{ij}^{l}(t)$ is assumed activity of plasticity-related factors (e.g. Calmodulin), which has similar dynamics to the synaptic conductance $g_{ij}(t)$ but with a longer decay time constant τ_l compared to the voltage change. The coincident detection was implemented by multiplying the place cell input $I_{p,i}^{exc}(t)$ from DG with $s_j(t)$. Self-connections were excluded, meaning that $w_{ij}^{rec} = 0$ (if $i = j$).

The regularization rule was modeled as

$$w_{ij}^{rec} \leftarrow w_{ij}^{rec} \cdot (a_{tot}^{rec} / \sum_j w_{ij}^{rec})$$

, where a_{tot}^{rec} is the gain of the regularization, by which the regularization rule ensures that the summation of the postsynaptic weights is always restricted.

The parameter values used in this model are summarized in Table 1.

Parameter name	**Symbol**	**Value**	**Parameter name**	**Symbol**	**Value**
Number of trials	N_{trial}	10	<u>Synapse</u>		
Time of one trial	T	12000 ms	Reversal potential (Exc)	E_{ampa}	0
Time derivative	dt	0.5 ms	Reversal potential (Inh)	E_{gaba}	-65
<u>CA3 excitatory neural unit</u>			Time constant (Exc)	τ_{ampa}	10 ms
Number of units	N^{exc}	8	Time constant (Inh)	τ_{gaba} τ_{gaba}	20 ms
Parameters of Izhikevich model	C^{exc}	50	Synaptic weight (CA3 Inh → CA3 Exc)	w^{ie}	1
	k^{exc}	0.5	Synaptic weight (CA3 Exc → CA3 Inh)	w^{ei}	1
	v_r^{exc}	-60	Synaptic weight	w^{pe}	1 ($i = j$) or 0 (

			(DG → CA3 Exc)		$i \neq j$ for CA3 exc unit i and DG j)
	v_t^{exc}	-45	Synaptic weight (MS → CA3 Inh)	w^{ti}	1
	v_{peak}^{exc}	40	<u>External Input</u>		
	a^{exc}	0.02	Amplitude of place input	a_p	30
	b^{exc}	-0.5	Peak position of place input	x_{peak}	2, 3, 4, 5 cm
	c^{exc}	-45	Window width of place input	σ_p	1 cm
	d^{exc}	50	Amplitude of theta input	a_{th}	-80
<u>CA3 Inhibitory neural unit</u>			Frequency of theta input	f_{th}	7 Hz
Number of units	N^{inh}	1	Baseline of excitatory input	I_{base}^{exc}	20
Parameters of Izhikevich model	C^{inh}	20	Baseline of inhibitory input	I_{base}^{inh}	100
	k^{inh}	1	Noise level of excitatory input	σ_{noise}^{exc}	0
	v_r^{inh}	-55	Noise level of inhibitory input	σ_{noise}^{inh}	0
	v_t^{inh}	-40	<u>Plasticity</u>		
	v_{peak}^{inh}	25	Learning rate for Hebbian plasticity	a_{Hebb}	0.0083 (100/T)
	a^{inh}	0.2	Synaptic time constant for learning	τ_l	300 ms
	b^{inh}	0.025	Summation limit for regularization	a_{tot}^{rec}	1
	c^{inh}	-45	Velocity in place	–	1 cm/s
	d^{inh}	20			

Table 1. Parameters of the small CA3 model (values are for Figure 1-4)

Resting session

In the resting session, we removed the external place and theta inputs and added independent noise inputs into each CA3 excitatory unit to induce spontaneous spiking. In addition, the

synaptic plasticity was also turned off. The specific parameter changes for the resting session are as follows:
$I_{base}^{exc} = 24.4$, $I_{base}^{inh} = 60$, $a_{th} = 0$, $a_p = 0$, $\sigma_{noise}^{exc} = 10$, $a_{Hebb} = 0$.

Altered models

For the model with self-connections in the recurrent synapse (Figure 4—figure supplement 1), we set $w_{ij}^{rec} \neq 0 (i = j)$, which were excluded in the original model.

For the model without coincident detection (Figure 4—figure supplement 2), we replaced $dg_{ij}^{l}(t)$ as
$dg_{ij}^{l}(t) = -g_{ij}^{l}(t-1)/\tau_l + s_j(t)$.
We set $a_{Hebb} = 0.083$ (10 times larger) for a larger learning rate (Figure 4—figure supplement 2 F-J).

For the model with a shorter learning time constant (Figure 4—figure supplement 3), we set $\tau_l = 20$ ms and set $a_{Hebb} = 0.083$ for a larger learning rate (Figure 4—figure supplement 3 F-J).

For the model without theta input from MS (Figure 4—figure supplement 4), we set $a_{th} = 0$ and $I_{base}^{inh} = 60$.

Other settings and processes were the same as in the small CA3 model (Figure 1-4).

Large Model

In the large model, the synaptic connections between the CA3 circuit units were modeled as probabilistic, reflecting that the actual connections in the CA3 circuit are not predetermined (Rebola et al., 2017). The simulation of the large model was done using Brian2 neural simulator (Stimberg et al., 2019). The number of CA3 excitatory units was $N_{exc} = 800$, and the number of CA3 inhibitory units was $N_{inh} = 200$. The probability of the DG (place input)-CA3 excitatory connection was $p_{pe} = 0.005$ (Claiborne et al., 1986; Rebola et al., 2017), the CA3 excitatory-CA3 excitatory recurrent connection was $p_{rec} = 0.1$ (Guzman et al., 2016), the CA3 inhibitory-CA3 excitatory connection was $p_{ie} = 0.25$, the CA3 excitatory-CA3 inhibitory connection was $p_{ei} = 0.25$, and the MS (theta input)-CA3 inhibitory connection was $p_{ti} = 1$. These probabilities were based on (Ecker et al., 2022; Rebola et al., 2017). The synaptic weights were adjusted with $w_{ij}^{pe} = 10$ (if connected) and $a_{tot}^{rec} = 7$. The number of trials in the running session is three, and the resting session was performed before and after the running session. Other parameters were the same as in the small model.
In Figure 7H and L, 15 models were executed with different random seeds. Units for the phase precession analysis were selected based on two criteria: they responded to place input and exhibited an expansion of firing through learning (more than 0.2 sec earlier in the last trial than the first trial).

Theta phase precession

The local field potential (LFP) was calculated as the summation of the membrane potentials of all excitatory units. Next, the LFP signal was filtered using a bandpass filter (5-12 Hz), and a Hibert transform was applied. The phase component was extracted from the transformed signal. Finally, a linear regression analysis was applied to the plot of place vs phase to estimate the slope value.

Crosscorrelogram

The spike timing differences were collected for each unit pair (unit i and unit j, $i \neq j$). These timing differences were grouped based on the activation status of the units during the running session, whether both units were responded, one unit in the pair was responded while the other was not, or both units were non-responded. In the analysis of additional learning and relearning, pairs consisting of the initial and the new sequence sets were also plotted. The densities were calculated over a range of -600 to 600 ms.

Replay sequence

Linear regression was performed between the difference in peak positions of place inputs during learning and lags during replay after learning with a lag range from -200 to 200 ms of pairs between responded units. The unit responded to the first place input was excluded.

Dynamical analysis

The nullcline lines were defined as the points where the formulas (eq1) and (eq2) (for excitatory, eq3 instead of eq2 for inhibitory) were equal to 0. The nullclines were represented by the equations:

$u = k(v - v_r)(v - v_t) + I$ (v-nullcline)

$u = b(v - v_r)$ (u-nullcline)

The equilibrium points were determined as the intersection between the v-nullcline and the u-nullcline. The stability of each equilibrium point was determined by the eigenvalues of the Jacobian matrix of the system represented by the formulas (eq1) and (eq2). If the two eigenvalues are both negative, the equilibrium point is stable. Otherwise, it is unstable (Izhikevich, 2010). When the formulas (eq1) and (eq2) were redefined as:

$dv = V(v, u)$

$du = U(v, u)$

, the Jacobian matrix, L, was defined as:

$$L = \begin{pmatrix} a_L & b_L \\ c_L & d_L \end{pmatrix}$$

$a_L = \partial V / \partial v$

$b_L = \partial V / \partial u$

$c_L = \partial U / \partial v$

$d_L = \partial U / \partial u$.

The eigenvalues λ, and eigenvectors x, of the Jacobian matrix L can be computed by solving the equation:
$Lx = \lambda x$.

The eigenvalues can be obtained by solving the following equation:
$\lambda^2 - trL\lambda + detL = 0$
$trL = a_L + d_L$
$detL = a_L d_L - b_L c_L$.

For the equilibrium point to be stable, both eigenvalues should be negative, which corresponds to $trL < 0$ and $detL > 0$. If the conditions are not met, the equilibrium point is unstable.

The equilibrium points of excitatory units $\bar{v}^{exc}$ were obtained by solving the following equation:

$$\bar{v}^{exc} = \frac{b^{exc} \pm \sqrt{D}}{2k^{exc}} + \frac{v_r^{esc} + v_t^{esc}}{2}$$

$$D = b^{exc2} - 4k^{exc}(-k^{exc}(\frac{v_t^{exc} - v_r^{exc}}{2})^2 - b^{exc}\frac{v_t^{exc} - v_r^{exc}}{2} + I)$$

It exhibited a saddle-node bifurcation when the constant input current I was below 24.5. In this case, the negative side equilibrium was stable, while the positive side was unstable (Izhikevich 2010). The equilibrium points disappeared above 24.5.

Equilibrium points inhibitory units $\bar{v}^{inh}$ were obtained by solving for v in following equation:
$k(v - v_r^{inh})(v - v_t^{inh}) + I - B(v) = 0$ (see eq3)
, which was solved using scipy.optimize.fsolve method with a moving constant I.

It exhibited Andronov–Hopf bifurcation. Then, trL^{inh} and $detL^{inh}$ were

$$trL^{inh} = \frac{k^{inh}}{C^{inh}}(2\bar{v}^{inh} - v_r^{inh} - v_t^{inh}) - a^{inh}$$

$$detL^{inh} = \frac{a^{inh}}{C^{inh}}\{-k^{inh}(2\bar{v}^{inh} - v_r^{inh} - v_t^{inh}) + B'(\bar{v}^{inh})\}$$

$B'(\bar{v}^{inh}) = 0$ when $\bar{v}^{inh} < v_r^{inh}$ and $B'(\bar{v}^{inh}) = 3b^{inh}(\bar{v}^{inh} - v_r^{inh})^2$ when $\bar{v}^{inh} \geq v_r^{inh}$.
The equilibrium point was stable when $trL^{inh} \leq 0$ and unstable when $trL^{inh} > 0$, as $detL^{inh}$ is always positive. The bifurcation point occurred at I = 73.7.

Code Availability Statement

The scripts for this study can be found in the Google Colaboratory
https://colab.research.google.com/drive/1mwl6ti3lAFtVwtfoZBPhdbSUXrUoCd7v?usp=sharing

Acknowledgements

We thank Hiroyuki Miyawaki and Takuya Isomura for their valuable contributions to the discussion.

Author contributions

Conceptualization: SK; Investigation: SK; Visualization: SK; Supervision: KM; Writing—original; draft: SK; Writing—review & editing: SK, KM; Funding Acquisition: KM

Reference

August, D.A., Levy, W.B., 1999. Temporal sequence compression by an integrate-and-fire model of hippocampal area CA3. J. Comput. Neurosci. 6, 71–90.

Banino, A., Barry, C., Uria, B., Blundell, C., Lillicrap, T., Mirowski, P., Pritzel, A., Chadwick, M.J., Degris, T., Modayil, J., Wayne, G., Soyer, H., Viola, F., Zhang, B., Goroshin, R., Rabinowitz, N., Pascanu, R., Beattie, C., Petersen, S., Sadik, A., Gaffney, S., King, H., Kavukcuoglu, K., Hassabis, D., Hadsell, R., Kumaran, D., 2018. Vector-based navigation using grid-like representations in artificial agents. Nature 557, 429–433.

Barron, H.C., Reeve, H.M., Koolschijn, R.S., Perestenko, P.V., Shpektor, A., Nili, H., Rothaermel, R., Campo-Urriza, N., O'Reilly, J.X., Bannerman, D.M., Behrens, T.E.J., Dupret, D., 2020. Neuronal Computation Underlying Inferential Reasoning in Humans and Mice. Cell 183, 228–243.e21.

Bi, G.Q., Poo, M.M., 1998. Synaptic modifications in cultured hippocampal neurons: dependence on spike timing, synaptic strength, and postsynaptic cell type. J. Neurosci. 18, 10464–10472.

Brandalise, F., Gerber, U., 2014. Mossy fiber-evoked subthreshold responses induce timing-dependent plasticity at hippocampal CA3 recurrent synapses. Proc. Natl. Acad. Sci. U. S. A. 111, 4303–4308.

Buzsáki, G., 1986. Hippocampal sharp waves: their origin and significance. Brain Res. 398, 242–252.

Buzsáki, G., 2005. Theta rhythm of navigation: link between path integration and landmark navigation, episodic and semantic memory. Hippocampus 15, 827–840.

Buzsáki, G., 2015. Hippocampal sharp wave-ripple: A cognitive biomarker for episodic memory and planning. Hippocampus 25, 1073–1188.

Buzsáki, G., Leung, L.W., Vanderwolf, C.H., 1983. Cellular bases of hippocampal EEG in the behaving rat. Brain Res. 287, 139–171.

Carr, M.F., Karlsson, M.P., Frank, L.M., 2012. Transient slow gamma synchrony underlies hippocampal memory replay. Neuron 75, 700–713.

Cazin, N., Llofriu Alonso, M., Scleidorovich Chiodi, P., Pelc, T., Harland, B., Weitzenfeld, A., Fellous, J.-M., Dominey, P.F., 2019. Reservoir computing model of prefrontal cortex creates novel combinations of previous navigation sequences from hippocampal place-cell replay with spatial reward propagation. PLoS Comput. Biol. 15, e1006624.

Chadwick, A., van Rossum, M.C., Nolan, M.F., 2016. Flexible theta sequence compression mediated via phase precessing interneurons. Elife 5.

Chenani, A., Sabariego, M., Schlesiger, M.I., Leutgeb, J.K., Leutgeb, S., Leibold, C., 2019. Hippocampal CA1 replay becomes less prominent but more rigid without inputs from medial entorhinal cortex. Nat. Commun. 10, 1341.
Choi, J.-H., Sim, S.-E., Kim, J.-I., Choi, D.I., Oh, J., Ye, S., Lee, J., Kim, T., Ko, H.-G., Lim, C.-S., Kaang, B.-K., 2018. Interregional synaptic maps among engram cells underlie memory formation. Science 360, 430–435.
Claiborne, B.J., Amaral, D.G., Cowan, W.M., 1986. A light and electron microscopic analysis of the mossy fibers of the rat dentate gyrus. J. Comp. Neurol. 246, 435–458.
Courellis, H.S., Nummela, S.U., Metke, M., Diehl, G.W., Bussell, R., Cauwenberghs, G., Miller, C.T., 2019. Spatial encoding in primate hippocampus during free navigation. PLoS Biol. 17, e3000546.
Csicsvari, J., Hirase, H., Mamiya, A., Buzsáki, G., 2000. Ensemble patterns of hippocampal CA3-CA1 neurons during sharp wave-associated population events. Neuron 28, 585–594.
Davoudi, H., Foster, D.J., 2019. Acute silencing of hippocampal CA3 reveals a dominant role in place field responses. Nat. Neurosci. 22, 337–342.
Diba, K., Buzsáki, G., 2007. Forward and reverse hippocampal place-cell sequences during ripples. Nat. Neurosci. 10, 1241–1242.
Dragoi, G., Buzsáki, G., 2006. Temporal encoding of place sequences by hippocampal cell assemblies. Neuron 50, 145–157.
Dragoi, G., Tonegawa, S., 2011. Preplay of future place cell sequences by hippocampal cellular assemblies. Nature 469, 397–401.
Drieu, C., Zugaro, M., 2019. Hippocampal Sequences During Exploration: Mechanisms and Functions. Front. Cell. Neurosci. 13, 232.
Ecker, A., Bagi, B., Vértes, E., Steinbach-Németh, O., Karlócai, M.R., Papp, O.I., Miklós, I., Hájos, N., Freund, T.F., Gulyás, A.I., Káli, S., 2022. Hippocampal sharp wave-ripples and the associated sequence replay emerge from structured synaptic interactions in a network model of area CA3. Elife 11.
Eliav, T., Geva-Sagiv, M., Yartsev, M.M., Finkelstein, A., Rubin, A., Las, L., Ulanovsky, N., 2018. Nonoscillatory Phase Coding and Synchronization in the Bat Hippocampal Formation. Cell 175, 1119–1130.e15.
Enel, P., Procyk, E., Quilodran, R., Dominey, P.F., 2016. Reservoir Computing Properties of Neural Dynamics in Prefrontal Cortex. PLoS Comput. Biol. 12, e1004967.
Fernández-Ruiz, A., Oliva, A., Nagy, G.A., Maurer, A.P., Berényi, A., Buzsáki, G., 2017. Entorhinal-CA3 Dual-Input Control of Spike Timing in the Hippocampus by Theta-Gamma Coupling. Neuron 93, 1213–1226.e5.
Foster, D.J., Wilson, M.A., 2006. Reverse replay of behavioural sequences in hippocampal place cells during the awake state. Nature 440, 680–683.
Freund, T.F., Antal, M., 1988. GABA-containing neurons in the septum control inhibitory interneurons in the hippocampus. Nature 336, 170–173.
Geisler, C., Diba, K., Pastalkova, E., Mizuseki, K., Royer, S., Buzsáki, G., 2010. Temporal delays among place cells determine the frequency of population theta oscillations in the hippocampus. Proc. Natl. Acad. Sci. U. S. A. 107, 7957–7962.
Glorot, X., Bordes, A., Bengio, Y., 2011. Deep Sparse Rectifier Neural Networks. In: Gordon, G., Dunson, D., Dudík, M. (Eds.), Part I: Notable Papers, Proceedings of Machine Learning Research. Presented at the International Conference on Artificial Intelligence and Statistics, Fort Lauderdale, FL, USA, pp. 315–323.
Gordon, B., 1988. Preserved learning of novel information in amnesia: evidence for multiple memory systems. Brain Cogn. 7, 257–282.
Guan, H., Middleton, S.J., Inoue, T., McHugh, T.J., 2021. Lateralization of CA1 assemblies in the absence of CA3 input. Nat. Commun. 12, 6114.
Guzman, S.J., Schlögl, A., Frotscher, M., Jonas, P., 2016. Synaptic mechanisms of pattern

completion in the hippocampal CA3 network. Science 353, 1117–1123.
Haga, T., Fukai, T., 2018. Recurrent network model for learning goal-directed sequences through reverse replay. Elife 7.
Haider, B., Häusser, M., Carandini, M., 2013. Inhibition dominates sensory responses in the awake cortex. Nature 493, 97–100.
Hájos, N., Karlócai, M.R., Németh, B., Ulbert, I., Monyer, H., Szabó, G., Erdélyi, F., Freund, T.F., Gulyás, A.I., 2013. Input-output features of anatomically identified CA3 neurons during hippocampal sharp wave/ripple oscillation in vitro. J. Neurosci. 33, 11677–11691.
Harris, K.D., Henze, D.A., Hirase, H., Leinekugel, X., Dragoi, G., Czurkó, A., Buzsáki, G., 2002. Spike train dynamics predicts theta-related phase precession in hippocampal pyramidal cells. Nature 417, 738–741.
Henze, D.A., Urban, N.N., Barrionuevo, G., 2000. The multifarious hippocampal mossy fiber pathway: a review. Neuroscience 98, 407–427.
Henze, D.A., Wittner, L., Buzsáki, G., 2002. Single granule cells reliably discharge targets in the hippocampal CA3 network in vivo. Nat. Neurosci. 5, 790–795.
Hwaun, E., Colgin, L.L., 2019. CA3 place cells that represent a novel waking experience are preferentially reactivated during sharp wave-ripples in subsequent sleep. Hippocampus 29, 921–938.
Izhikevich, E.M., 2010. Dynamical Systems in Neuroscience: The Geometry of Excitability and Bursting (Computational Neuroscience) by Izhikevich, Eugene M. (2010) (Computational Neuroscience Series). The MIT Press.
Jaeger, H., Haas, H., 2004. Harnessing nonlinearity: predicting chaotic systems and saving energy in wireless communication. Science 304, 78–80.
Jahnke, S., Timme, M., Memmesheimer, R.-M., 2015. A Unified Dynamic Model for Learning, Replay, and Sharp-Wave/Ripples. J. Neurosci. 35, 16236–16258.
Jensen, O., Idiart, M.A., Lisman, J.E., 1996. Physiologically realistic formation of autoassociative memory in networks with theta/gamma oscillations: role of fast NMDA channels. Learn. Mem. 3, 243–256.
Jensen, O., Lisman, J.E., 1996. Theta/gamma networks with slow NMDA channels learn sequences and encode episodic memory: role of NMDA channels in recall. Learn. Mem. 3, 264–278.
Johnson, A., Redish, A.D., 2007. Neural ensembles in CA3 transiently encode paths forward of the animal at a decision point. J. Neurosci. 27, 12176–12189.
Kamondi, A., Acsády, L., Wang, X.J., Buzsáki, G., 1998. Theta oscillations in somata and dendrites of hippocampal pyramidal cells in vivo: activity-dependent phase-precession of action potentials. Hippocampus 8, 244–261.
Karlsson, M.P., Frank, L.M., 2009. Awake replay of remote experiences in the hippocampus. Nat. Neurosci. 12, 913–918.
King, C., Recce, M., O'Keefe, J., 1998. The rhythmicity of cells of the medial septum/diagonal band of Broca in the awake freely moving rat: relationships with behaviour and hippocampal theta. Eur. J. Neurosci. 10, 464–477.
Laje, R., Buonomano, D.V., 2013. Robust timing and motor patterns by taming chaos in recurrent neural networks. Nat. Neurosci. 16, 925–933.
London, M., Häusser, M., 2005. Dendritic computation. Annu. Rev. Neurosci. 28, 503–532.
Mehta, M.R., Lee, A.K., Wilson, M.A., 2002. Role of experience and oscillations in transforming a rate code into a temporal code. Nature 417, 741–746.
Mehta, M.R., Quirk, M.C., Wilson, M.A., 2000. Experience-dependent asymmetric shape of hippocampal receptive fields. Neuron 25, 707–715.
Miconi, T., 2017. Biologically plausible learning in recurrent neural networks reproduces neural dynamics observed during cognitive tasks. Elife 6.
Middleton, S.J., McHugh, T.J., 2016. Silencing CA3 disrupts temporal coding in the CA1

ensemble. Nat. Neurosci. 19, 945–951.
Mishra, R.K., Kim, S., Guzman, S.J., Jonas, P., 2016. Symmetric spike timing-dependent plasticity at CA3–CA3 synapses optimizes storage and recall in autoassociative networks. Nat. Commun. 7, 11552.
Miyawaki, H., Diba, K., 2016. Regulation of Hippocampal Firing by Network Oscillations during Sleep. Curr. Biol. 26, 893–902.
Mizuseki, K., Royer, S., Diba, K., Buzsáki, G., 2012. Activity dynamics and behavioral correlates of CA3 and CA1 hippocampal pyramidal neurons. Hippocampus 22, 1659–1680.
Nicola, W., Clopath, C., 2019. A diversity of interneurons and Hebbian plasticity facilitate rapid compressible learning in the hippocampus. Nat. Neurosci. 22, 1168–1181.
O'Keefe, J., Dostrovsky, J., 1971. The hippocampus as a spatial map. Preliminary evidence from unit activity in the freely-moving rat. Brain Res. 34, 171–175.
O'keefe, J., Nadel, L., 1978. The hippocampus as a cognitive map. Oxford university press.
O'Keefe, J., Recce, M.L., 1993. Phase relationship between hippocampal place units and the EEG theta rhythm. Hippocampus 3, 317–330.
Oliva, A., Fernández-Ruiz, A., Buzsáki, G., Berényi, A., 2016. Spatial coding and physiological properties of hippocampal neurons in the Cornu Ammonis subregions. Hippocampus 26, 1593–1607.
O'Neill, J., Senior, T.J., Allen, K., Huxter, J.R., Csicsvari, J., 2008. Reactivation of experience-dependent cell assembly patterns in the hippocampus. Nat. Neurosci. 11, 209–215.
Petsche, H., Stumpf, C., Gogolak, G., 1962. [The significance of the rabbit's septum as a relay station between the midbrain and the hippocampus. I. The control of hippocampus arousal activity by the septum cells]. Electroencephalogr. Clin. Neurophysiol. 14, 202–211.
Qasim, S.E., Fried, I., Jacobs, J., 2021. Phase precession in the human hippocampus and entorhinal cortex. Cell 184, 3242–3255.e10.
Rebola, N., Carta, M., Mulle, C., 2017. Operation and plasticity of hippocampal CA3 circuits: implications for memory encoding. Nat. Rev. Neurosci. 18, 208–220.
Reifenstein, E.T., Bin Khalid, I., Kempter, R., 2021. Synaptic learning rules for sequence learning. Elife 10.
Rogerson, T., Cai, D.J., Frank, A., Sano, Y., Shobe, J., Lopez-Aranda, M.F., Silva, A.J., 2014. Synaptic tagging during memory allocation. Nat. Rev. Neurosci. 15, 157–169.
Romani, S., Tsodyks, M., 2015. Short-term plasticity based network model of place cells dynamics. Hippocampus 25, 94–105.
Schlesiger, M.I., Cannova, C.C., Boublil, B.L., Hales, J.B., Mankin, E.A., Brandon, M.P., Leutgeb, J.K., Leibold, C., Leutgeb, S., 2015. The medial entorhinal cortex is necessary for temporal organization of hippocampal neuronal activity. Nat. Neurosci. 18, 1123–1132.
Schlingloff, D., Káli, S., Freund, T.F., Hájos, N., Gulyás, A.I., 2014. Mechanisms of sharp wave initiation and ripple generation. J. Neurosci. 34, 11385–11398.
Scoville, W.B., Milner, B., 1957. Loss of recent memory after bilateral hippocampal lesions. J. Neurol. Neurosurg. Psychiatry 20, 11–21.
Sharif, F., Tayebi, B., Buzsáki, G., Royer, S., Fernandez-Ruiz, A., 2021. Subcircuits of Deep and Superficial CA1 Place Cells Support Efficient Spatial Coding across Heterogeneous Environments. Neuron 109, 363–376.e6.
Silva, D., Feng, T., Foster, D.J., 2015. Trajectory events across hippocampal place cells require previous experience. Nat. Neurosci. 18, 1772–1779.
Skaggs, W.E., McNaughton, B.L., Wilson, M.A., Barnes, C.A., 1996. Theta phase precession in hippocampal neuronal populations and the compression of temporal sequences. Hippocampus 6, 149–172.
Stimberg, M., Brette, R., Goodman, D.F., 2019. Brian 2, an intuitive and efficient neural simulator. Elife 8.
Sussillo, D., Abbott, L.F., 2009. Generating coherent patterns of activity from chaotic neural

networks. Neuron 63, 544–557.
Suzuki, S.S., Smith, G.K., 1988. Spontaneous EEG spikes in the normal hippocampus. III. Relations to evoked potentials. Electroencephalogr. Clin. Neurophysiol. 69, 541–549.
Tolman, E.C., 1948. Cognitive maps in rats and men. Psychol. Rev. 55, 189–208.
Tsodyks, M.V., Skaggs, W.E., Sejnowski, T.J., McNaughton, B.L., 1996. Population dynamics and theta rhythm phase precession of hippocampal place cell firing: a spiking neuron model. Hippocampus 6, 271–280.
Wang, J.X., Kurth-Nelson, Z., Kumaran, D., Tirumala, D., Soyer, H., Leibo, J.Z., Hassabis, D., Botvinick, M., 2018. Prefrontal cortex as a meta-reinforcement learning system. Nat. Neurosci. 21, 860–868.
Yamamoto, J., Tonegawa, S., 2017. Direct Medial Entorhinal Cortex Input to Hippocampal CA1 Is Crucial for Extended Quiet Awake Replay. Neuron 96, 217–227.e4.
Yassa, M.A., Stark, C.E.L., 2011. Pattern separation in the hippocampus. Trends Neurosci. 34, 515–525.
Zutshi, I., Brandon, M.P., Fu, M.L., Donegan, M.L., Leutgeb, J.K., Leutgeb, S., 2018. Hippocampal Neural Circuits Respond to Optogenetic Pacing of Theta Frequencies by Generating Accelerated Oscillation Frequencies. Curr. Biol. 28, 1179–1188.e3.